J. Fluid Mech. (2005), *vol.* 538, *pp.* 399–428.
doi:10.1017/S0022112005005537 Printed in the United Kingdom

Granular collapse in two dimensions

By N. J. BALMFORTH[1] AND R. R. KERSWELL[2]

[1]Departments of Mathematics and Earth and Ocean Science, UBC, Vancouver

[2]Department of Mathematics, University of Bristol, UK

(Received 22 November 2004 and in revised form 8 March 2005)

An experimental investigation is conducted into the collapse of granular columns inside rectangular channels. The final shape is documented for slumps inside relatively wide channels, and for collapses inside much narrower slots. In both cases, the collapse is initiated by withdrawing a swinging gate or sliding door, and the flow remains fairly two-dimensional. Four different granular media are used; the properties of the materials vary significantly, notably in their angles of friction for basal sliding and internal deformation. If H is the initial height of the column, h_∞ the maximum final height of the column and a the initial aspect ratio, then the data suggest that $H/h_\infty \sim a^{0.6}$ in wide channels and $H/h_\infty \sim a^{0.5}$ for narrow slots. For the runout, we find that $(l_\infty - L)/L \sim a^{0.9\pm0.1}$ for wide channels, and $(l_\infty - L)/L \sim a^{0.65\pm0.05}$ or $l_\infty/L \sim a^{0.55\pm0.05}$ for narrow slots, where l_∞ is the maximum runout of the material and L the initial length of the column along the channel ($a := H/L$). In all cases, the numerical constant of proportionality in these scaling relations shows clear material dependence. In wide slots, there is no obvious universal scaling behaviour of the final profile, but such a behaviour is evident in narrow slots. The experimental results are compared with theoretical results based on a shallow granular-flow model. The qualitative behaviour of the slump in the wide slot is reproduced by the theoretical model. However, there is qualitative disagreement between theory and the experiments in the narrow slot because of the occurrence of secondary surface avalanching.

1. Introduction

The collapse and slump of a granular medium play a key role in a variety of physical settings in engineering and geophysics. Indeed, it is hard to overstate the significance in many costly industrial processes and environmental hazards. Yet, despite the importance, our understanding of the simplest kinds of granular flow remains incomplete. From the theoretical perspective, this is largely due to the lack of an acceptable continuum model for a granular material under the relevant physical conditions. However, until fairly recently it has also been the case that there have been relatively few experiments conducted to observe the slump of a suddenly released granular pile on a horizontal surface.

For these reasons, we explore one of the simplest kinds of flow configuration in this kind of medium: the granular 'dam-break' problem. This configuration has developed into a classical problem in fluid mechanics owing to its intrinsic interest, reproducibility in the laboratory and, at least in the two-dimensional case, accessibility on the theoretical side (e.g. Whitham 1974). The purpose of the current paper and a companion paper (Kerswell 2005) is to follow a parallel path for the granular dam breaks; we perform some experiments and compare the results with a simple theoretical

model. The current article focuses on the laboratory experiments and comparison; Kerswell (2005) describes in more detail the solution of the theoretical model.

Previous experimental work on related problems includes the releases of cylindrical piles by Lajeunesse, Mangeney-Castelnau & Vilotte (2004) and Lube *et al.* (2004). Neither work attempts a detailed comparison with a theoretical model. Instead, they opt for qualitative discussion of the observed dynamics and the construction of scaling laws for how the final shape depends on the initial height of the cylindrical column. Despite the complicated flow dynamics, both groups report simple scaling laws for the final maximum height and radius of the deposit. The question of whether such laws carry over in some straightfoward fashion to planar slumps in channels has also motivated the current work. In fact, we report some similar findings. A comparison of these existing experimental results with the axisymmetric version of the theory is given by Kerswell (2005).

The theoretical model we use treats the granular medium as a two-dimensional shallow fluid layer that slides over the plane beneath with relatively little internal shear. Basal friction then plays a key role in the dynamics. The model has much in common with that proposed by Savage & Hutter (1989 and elaborated on further by Savage & Hutter 1991; Hutter & Koch 1991; Hutter *et al.* 1995; Pouliquen & Forterre 2002), who explored the acceleration of granular layers on inclined surfaces, and has the same philosophical foundation as the St Venant model of fluid mechanics. The St Venant model is derived adopting a crude closure for the stresses in a turbulent water course, and has a mainly empirical justification. By contrast, the granular model used here can be formally derived by asymptotic means from the governing equations if the medium is assumed to be a fluid with a certain constitutive law for the internal stresses and sliding law at its base (we give this derivation in Appendix A). Unfortunately, this cannot be taken as a formal justification of the model because the original governing equations are in question in this instance. Nevertheless, we regard the derivation as a useful addition to the literature since it offers a means to generalize the theory to different physical situations (such as a sliding mass in a narrow slot, as described in Appendix B), connects the model with related theories used elsewhere (as in ice flow dynamics and viscoplastic fluid mechanics), and allows us to assess the physical conditions under which the model should remain valid (see Appendix A).

Experiments on approximately two-dimensional slumps have also been performed by Siavoshi & Kudrolli (2005), Lube *et al.* (2005) and Lajeunesse, Monnier & Homsy (2005), and further theoretical discussion has been offered by Staron & Hinch (2005) and Larrieu, Staron & Hinch (2005). Siavoshi & Kudrolli (2005) make a careful study of magnetically released granular steps over rough surfaces, thereby eliminating any influence of the detailed initiation of the slump. They focus on relatively shallow initial steps and present results on the internal dynamics, making a comparison with the phenomenological 'BCRE' model (Bouchaud *et al.* 1994) which crudely accounts for a superficial layer of avalanching grains. Our own experiments span a much wider range of the initial aspect ratio (height of the column divided by initial length along the channel), and we observe fast sliding granular gravity currents when the initial column is relatively high. These currents look plausibly as if largely plug-like flows, and so we have elected to compare the experiments with a shallow-fluid model of a sliding granular mass. Larrieu *et al.* (2005) expand further on such a description, although it is clearly limited for lower initial aspect ratios where superficial flow is certainly present. A rather different, but complementary, approach is taken by Staron & Hinch (2005) who evolve slumps via particle mechanics, assuming frictional rigid collisions between grains.

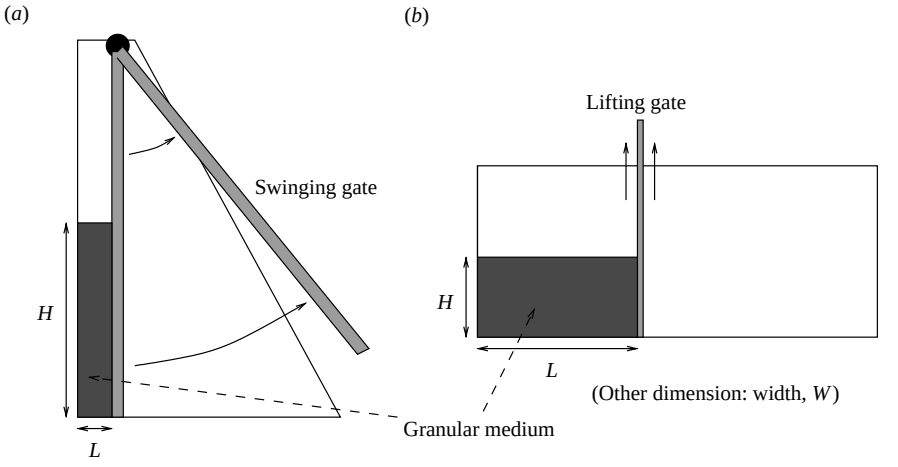

FIGURE 1. Sketches of the two experimental configurations. (*a*) Slot. (*b*) Box.

2. Experimental details

2.1. *The apparatus*

The slumps are performed in two different experimental set-ups (see figures 1 and 2):

(a) A Perspex slot with a swinging gate (the slot is triangular, with a height of 1 m at the hinge of the gate, some 75 cm long at the base, and has an adjustable width). The initial pile is put in place initially by funnelling the material into the slot from above. The metre-depth fall of the grains packs the initial pile relatively tightly, and in much the same way for each slump.

(b) A Perspex box with a sliding gate (dimensions 18 cm by 30 cm by 45 cm, with the gate positioned 20 cm along the 45 cm edge). The initial pile was formed by rocking the box back and forth and the packing is less tight than in the slot.

In each case, the apparatus initiates a dam break in a channel with rectangular cross-section. The initial granular pile has dimensions (H, L, W), where H is the depth, L is the length along the channel and W is its width. All are parameters that we vary in the experiment. For the slot, the width W could be set so that the slot was relatively narrow (1 cm) or wide (20 cm); the rectangular box could rotated to allow two width settings (18 cm and 30 cm). Most of our results relate to the slot with swinging gate.

2.2. *Materials*

We used four different granular media (figure 3):

(i) Grit, of irregular shape, but overall mean size of about 1 mm. Density: 2.6 g cm^{-3}. Approximate volume fraction: 0.54 loose, 0.59 packed.

(ii) Glass beads (ballotini) of mean diameter 0.8 mm – *fine glass.* Density: 2.5 g cm^{-3}. Approximate volume fraction: 0.58 loose, 0.63 packed.

(iii) Glass beads (ballotini) of mean diameter 3 mm – *coarse glass.* Density: 2.5 g cm^{-3}. Approximate volume fraction: 0.58 loose, 0.65 packed.

(iv) Polystyrene balls of mean diameter 0.75 mm. Density: 0.9 g cm^{-3}. Approximate volume fraction: 0.66 loose, 0.7 packed.

Most of the experiment, results were obtained using grit and fine glass. For all of the materials, we attempted to characterize the frictional properties in terms of

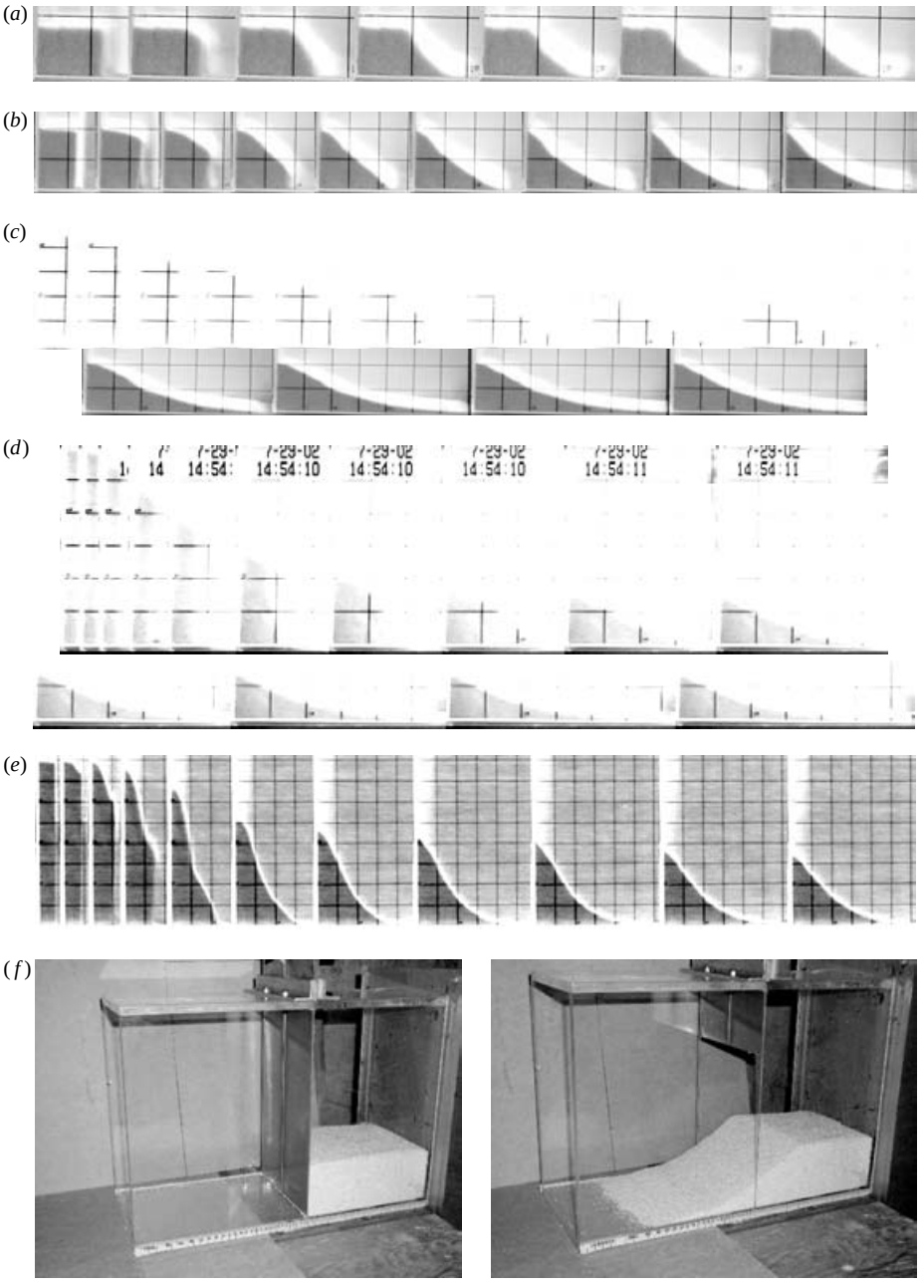

FIGURE 2. Photographs of collapses of columns of grit. Slumps in the wide slot ($W = 20\,\text{cm}$): (*a*) 'fractured' slump with $L = 6\,\text{cm}$ and $H = 4\,\text{cm}$. (*b*) $L = 6\,\text{cm}$ and $H = 10\,\text{cm}$. (*c*) $L = 5$ and $H = 24\,\text{cm}$. (*d*) Relatively rapid collapse with $L = 2\,\text{cm}$ and $H = 30\,\text{cm}$. Each image is $2/25\,\text{s}$ apart. Note that the line of sight of the camera is slightly inclined so that the brightly lit top surface of the deposit is also visible (and illustrates how the slump is largely two-dimensional). (*e*) Slump in the narrow slot: $L = 4\,\text{cm}$, $H = 40\,\text{cm}$ and $W = 1\,\text{cm}$. Each image is $4/25\,\text{s}$ apart, save for the last three, which are separated by $8/25\,\text{s}$ (and in which the majority of motion is in the form of an avalanching superficial flow). The grid shows squares of length 5 cm drawn on the outside of the slot which assist the measurement of depth (performed directly through the sidewall). (*f*) Slump in the box: two images, before and after, with $L = 20\,\text{cm}$, $H = 10\,\text{cm}$ and $W = 18\,\text{cm}$. Again, the inclined camera illustrates the two-dimensionality of the deposit.

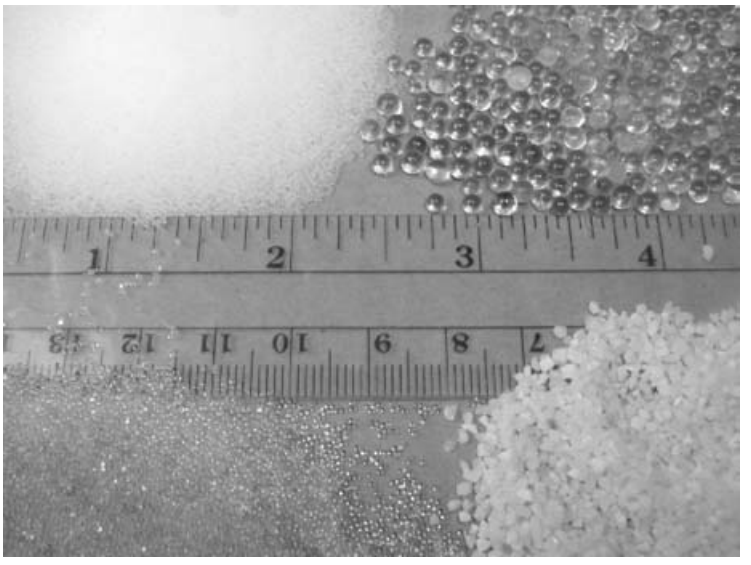

FIGURE 3. Photograph of the four granular materials. From top left and clockwise; polystyrene balls, coarse glass, grit and fine glass.

	δ (deg.)	ϕ (deg.)
Grit	18.5 ± 1.5	36.5 ± 4.5
Fine glass	14.75 ± 0.5	24.5 ± 2
Coarse glass	15 ± 2	26 ± 6
Polystyrene	15 ± 1	25.5 ± 2

TABLE 1. Results for 'bed' angle of friction, δ, and 'internal' angle of friction, ϕ.

two angles: the 'bed' angle of friction, δ, indicating how easily material slides over the smooth plate beneath, and the 'internal' angle of friction, ϕ, which measures how layers of the medium slide over one another. The results, which comprise a key ingredient in the theoretical model of § 6 and Appendix A, are summarized in table 1.

The bed angle of friction was estimated (following Hutter & Koch 1991) by determining when a rigid block of particles held together within a paper cylinder would begin to slide on an inclined surface made of the same material as the Perspex slot or box. The internal angle of friction was estimated by gluing particles to a plane whose inclination was raised until motion downslope began in an overlying granular layer. This angle was further compared with angles of repose measured from the final slopes of wedge-shaped piles that either avalanched to rest or were built up by deposition. There was substantial scatter in the data (notably in ϕ) which illustrates a known feature of granular medium, namely that sliding or avalanching begin and end at slightly different angles (reflecting in some way the difference between dynamic and static friction). We ignore such subdivisions here and pick the representative values in table 1 for ϕ and δ, which seems justified given the qualitative, but not quantitative, agreement between the theory and experiments outlined in the following sections.

The data reveal one significant feature of the four media: the polystyrene and glass beads are all fairly spherical and have similar bed and internal angles of friction. The

grit, on the other hand, is composed of angular rough particles and the corresponding friction angles are significantly higher.

Finally, we note that the slumps were performed in an air-conditioned laboratory maintained at 21 °C with humidity controlled at 46%. The granular materials were kept dry in this environment; moistening the materials or the sides of the channel even a small amount leads to markedly different results.

3. Phenomenology of the collapse

The phenomenology of the slumping process depends strongly on the initial aspect ratio a ($a := H/L$; see figure 1) of the column, as found for axisymmetric collapses by Lajeunesse *et al.* (2004) and Lube *et al.* (2004), and in the particle mechanics computations of Staron & Hinch (2005). There is a gradual transition from relatively slow fracturing avalanches of shallow columns to violent cascading collapses of tall columns (see figure 2). The shallowest initial piles develop fracture planes along which material slides down, and below which grains barely participate in the collapse, if at all (see the first row of images in figure 2). This flow structure was evident in video images taken through the sidewalls, and is explored in more detail in the experiments of Siavoshi & Kudrolli (2005). As the aspect ratio of the initial pile increases, less of the material resides in place, and eventually the whole pile participates in the collapse (second and subsequent experiments in figure 2). When a becomes large, the initial phases of collapse become fast, with the entire column appearing to expand sideways whilst collapsing downwards ballistically. On impacting the base and re-compacting, the material forms a denser mass that adjusts more slowly into a final equilibrium shape near the end of the slot. Simultaneously, a sliding current forms at the nose of the deposit that determines the run-out.

We use the final slumped profiles of the deposits as the main descriptor of the collapse. In all the geometries, variations in the direction across the channel were relatively slight (e.g. see figure 1). Thus, the deposit could be characterized by the thickness or depth h as a function of distance x down the slot. Before describing the experimental results in detail, we first compare the final profiles of a number of equivalent collapses to judge the reproducibility of the experiments (figure 4). The comparisons show profiles in the swinging slot; the profiles from the box were typically more reproducible (compared to the wide slot), at least for the initial configurations we used. In certain of the comparisons shown in figure 4, exactly the same material was tested in sequential experiments. In other cases, different batches of material were used at different points during the entire experimental sequence.

The final shapes are fairly reproducible, but not perfectly so. Some of the disagreement arises because the experiments did not have exactly the same amount of material (it is difficult to fill the slot with exactly the same amount of material because the particles can be packed differently, the gate does not fit exactly back in the same position after each release and the Perspex walls can deform outwards slightly). However, in the wider slot, there was also some effect of differences in the gate release, especially for the lighter particles (with the polystyrene balls, a vortex in the air trailing the gate can interact with the particles), and because the slump was not perfectly two-dimensional. To try to eliminate the peculiarities of particular releases, when we present data in the following sections, we combine multiple final profiles into averages whenever available. For the slumps in the wider slot, we also attempted to minimize any three-dimensional effects by combining measurements from both walls. Nevertheless, the comparisons in figure 4 illustrate one important aspect of the

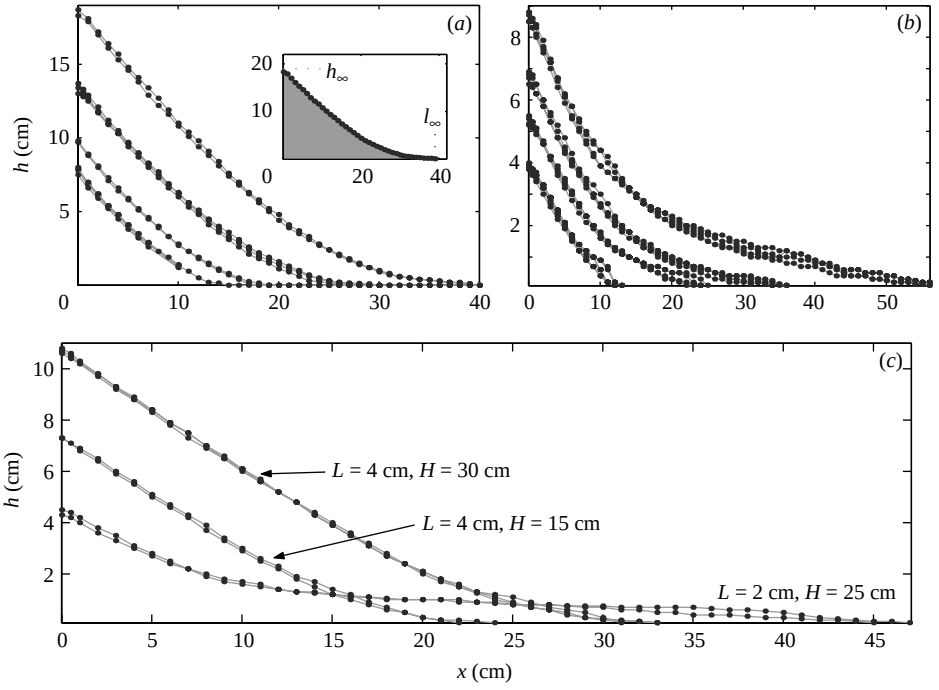

FIGURE 4. Reproducibility of the final profiles. (*a*) Grit, $L = 4$ cm, narrow: four sets of experimental slumps in the narrow slot with $H = 50$ cm (2 slumps), $H = 30$ cm (3 slumps), $H = 10$ cm (2 slumps) and $H = 7.5$ cm (3 slumps). (*b*) Grit: four sets of slumps in the wide slot with $H = 40$ cm (4 slumps), $H = 30$ cm (4 slumps), $H = 20$ cm (4 slumps) and $H = 10$ cm (4 slumps). (*c*) Fine glass: three sets of slumps with $H = 30$ cm (narrow slot, 3 slumps), $H = 15$ cm (narrow slot, 2 slumps) and $H = 25$ cm (wide slot, 2 slumps).

experiments: errors in measuring the final depths were insignificant in comparison to the variations in profile between experiments. Consequently, because we did not perform a large number of experiments for each initial configuration, it is difficult to assess the overall errors which originate mainly from those variations. A conservative estimate of the error in depth is up to half a centimetre, whereas the corresponding error in horizontal length at fixed depth could be up to a couple of centimetres because of the tapering of the final deposit.

Figure 4(*a*) also illustrates the measurement of the final maximum height, h_∞ (which is invariably at the wall), and the maximum runout, l_∞, both of which we use later as convenient characterizations of the deposits. While the final maximum height of the deposit is clearly defined, the final runout is much more ambiguous. This is because the layer tapers to depths comparable to the particle diameter at its nose and a small number of particles actually become detached from the main deposit and scattered further ahead. The maximum range reached by these detached granules was very variable, whereas the range of the contiguous deposit was much more reproducible. Given this and the fact that the experiments were motivated by a desire to assess the continuum-like properties of the granular material, we took the runout to be the range of the contiguous deposit where the height had decreased below 2 mm. This was essentially two particle diameters for the materials (grit and fine glass) used to compile the runout data and hence seemed a reasonable point at which to assume the granules were no longer moving in contact with each other.

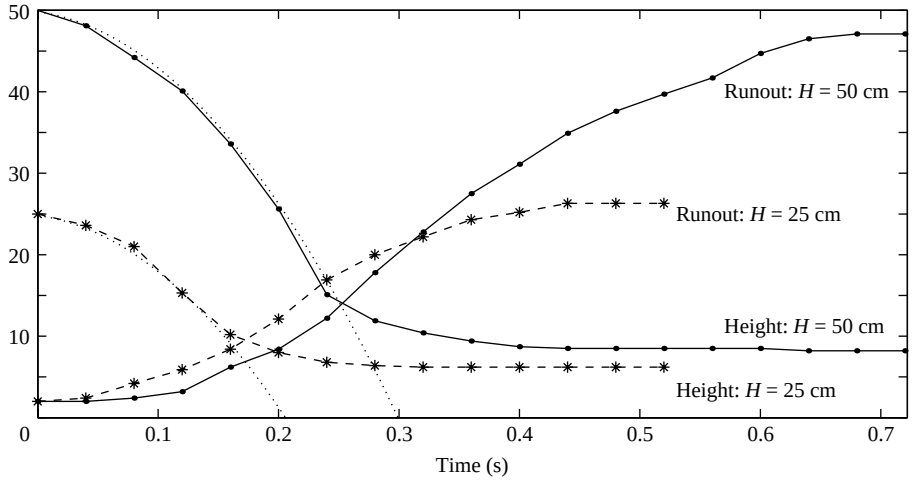

FIGURE 5. Time series showing the instantaneous maximum heights and runouts for two slumps of the grit in the wide slot with $L = 2$ cm ($H = 25$ cm and 50 cm). The dotted lines show the ballistic curve, $H - gt^2/2$.

Although we focus attention on the final profile as the descriptor of the collapse, figure 5 shows the dynamic evolution of h_∞ and l_∞ as a function of t for the grit in the wide slot. Two experiments are shown; the initial ballistic collapse is evident in this data, as is the more gradual deceleration. A more complete discussion of the evolutionary dynamics for fractured slumps is offered by Siavoshi & Kudrolli (2005). Collapses in the narrow slot show similar behaviour, although the ballistic fall appears to be distinctly delayed beyond the initial release of the gate, and the final adjustment to the ultimate deposit is noticeably different. More specifically, the wider slumps come to rest only when the sliding current at the nose of the deposit finally brakes to a halt. On the other hand, when the narrow slumps come to rest at the nose, material further back up the slot continues to adjust by the continual avalanching of superficial layers that decrease the surface slope until an equilibrium is reached.

4. Wide collapses

4.1. *Taller initial piles*

Experiments varying the initial length L and height H such that the overall volume of the initial column remained fixed are shown in figure 6 for the grit in the wide slot. The variance in the final shape illustrates how the slumped deposit is influenced by the initial aspect ratio in this geometry: the higher and narrower initial columns spread further and fall lower. A comparison of the initial and final areas indicates that there is also a change in packing: the initial area is systematically smaller than the final area (by what appears to be as much as 10% on occasions).† This change in packing is typical of slumps in the slot, and presumably reflects how the initial pile

† Note that the final depths and areas displayed in the figures are slightly overestimated: the slumps are not perfectly two-dimensional, and the final deposit is invariably slightly depressed in the middle of the channel compared to the walls, especially for the wide slot. Because measurements were taken directly through the sidewalls, the actual depths and areas, averaged across the slot, are therefore a little lower than those recorded.

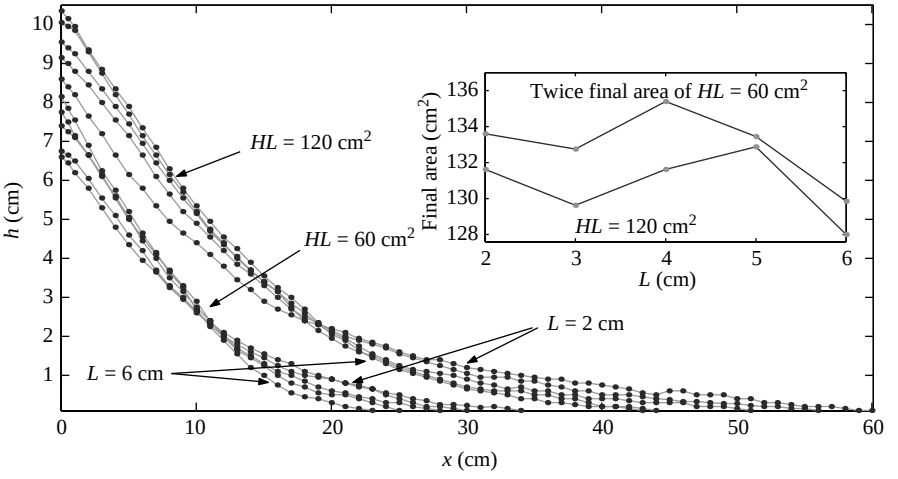

FIGURE 6. Final profiles: grit, varying initial length at fixed volume in a wide slot. The inset shows the measured final and initial areas.

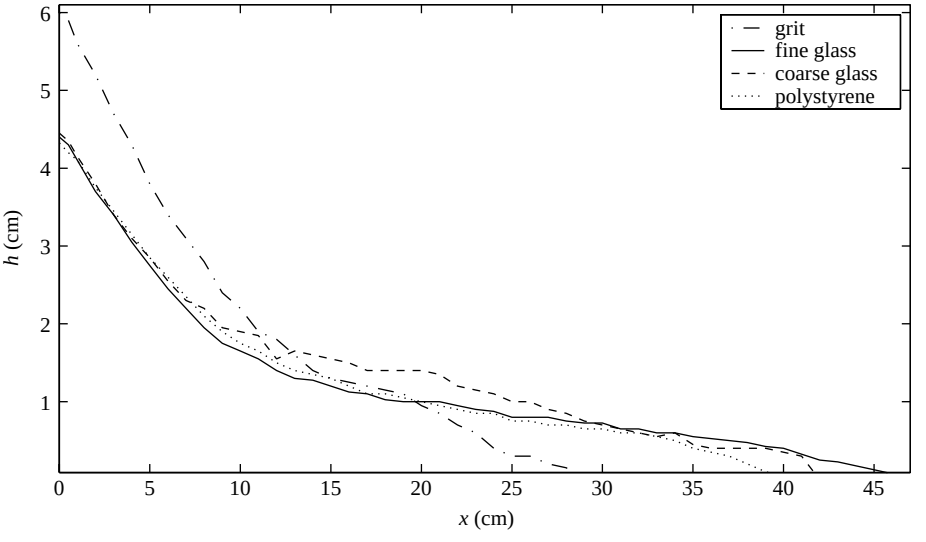

FIGURE 7. Final profiles for the four materials in the wide slot. $L = 2\,\text{cm}$ and $H = 25\,\text{cm}$.

is relatively closely packed by the method of filling, and the material expands on its way to the final deposit.

We compare final profiles for the four different granular materials in figure 7 for slumps with the same initial aspect ratio. Remarkably, three of the materials (fine glass, coarse glass and polystyrene) all slump to similar profiles, except nearer the nose of the deposit. However, the grit is noticeably different. Slumps in the box show the same trend even though the deposits are fractured, and final profiles of collapses of fine glass and polystyrene in the narrow slot are nearly indistinguishable and again unlike those of grit (slumps of the coarse glass are noticeably different in the narrow slot, but this is undoubtedly because the diameter of the spheres is not very different to the slot's width).

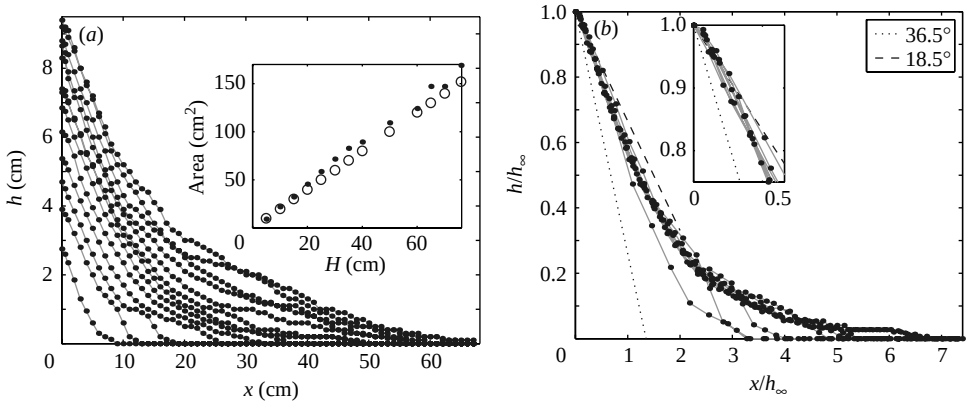

FIGURE 8. Final profiles for grit in the wide slot. (*a*) The 'raw' measurements of depth against distance from the end of the slot. The inset panel shows the recorded initial (○) and final (●) areas of the piles. (*b*) The profiles after lengths have been scaled by the maximum height of the final deposit (h_∞). The inset shows a magnification near the end of the slot.

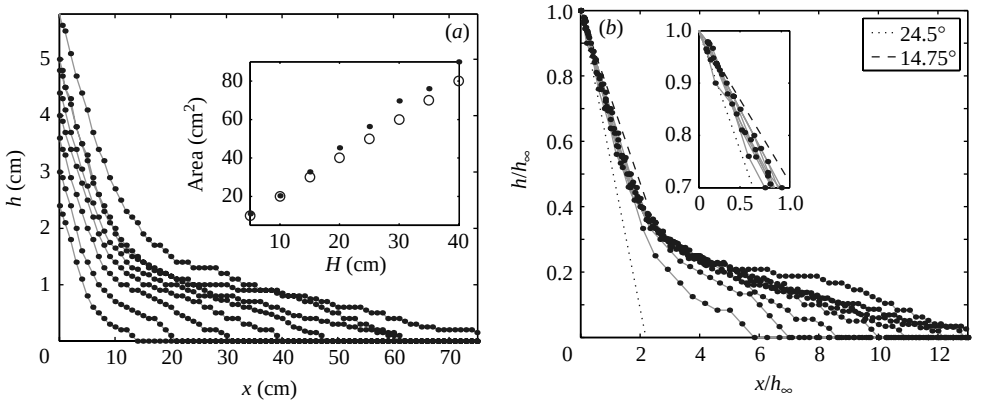

FIGURE 9. Similar to figure 8, but showing final profiles for fine glass in the wide slot.

A glance at the physical properties listed in § 2 indicates that, although the densities and particle diameters are quite different, the fine glass, coarse glass and polystyrene all have similar angles of friction; the corresponding angles for grit are distinctly higher. We conclude that friction plays a key role in determining the precise final shape of the deposit, which disagrees with the claims of Lube *et al.* (2004), but agrees with the results of Lajeunesse *et al.* (2004). The polystyrene balls also interact electrostatically with the Perspex walls of the slot: a small number of individual grains remain sticking to the walls of the channel above the main deposit at the end of the collapse. Nevertheless, the deposit remains fairly two-dimensional, and the slump as a whole appears to continue regardless of the additional electrostatic interaction with the walls. However, the polystyrene data were not used to extract scaling behaviour.

Figures 8 and 9 show a compendium of profiles from a series of experiments in which the initial length L of the pile was fixed, and the initial height H gradually increased. Although it does not seem possible to scale the profiles in such a way to collapse them all completely onto a common curve, there is some suggestion that a

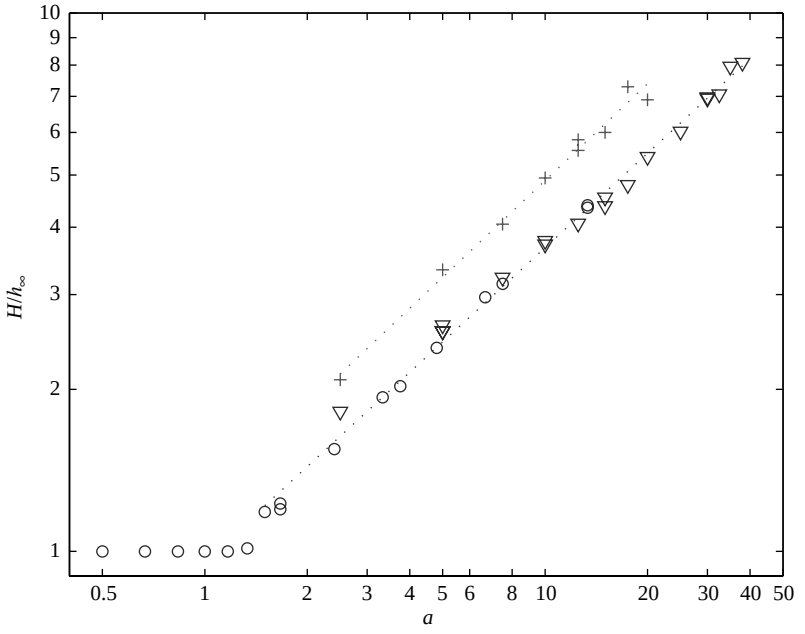

FIGURE 10. The initial to final height ratio H/h_∞ plotted against a for grit (○, $L > 2$; ▽, $L = 2$) and fine glass (+, all with $L = 2$ cm) in the wide slot. The dotted lines represent best fits through the data with gradients of 0.58 (grit) and 0.60 (fine glass).

scaling by the final, maximum height (i.e. h_∞) leads to a fairly compact description of the deposit. The rescaled profiles also indicate that the final deposits tend to decline from their maximum at the wall with nearly the same slope, and this slope is invariably the steepest over the whole deposit. The angle of the maximum slope lies between the internal and bed angles of friction, suggesting it is determined by a combination of both. Such combinations are, in fact, expected on theoretical grounds (§ 6). For grit, the maximum angle is about 23°, and for the fine glass it is about 18°.

Figure 10 illustrates our efforts to fit the ratio of initial to final heights, H/h_∞, by a simple power law in initial aspect ratio, a:

$$\frac{H}{h_\infty} \sim \lambda a^\alpha, \tag{4.1}$$

where $\alpha \approx 0.6$ for $a \geqslant 2$. Although the best-fit power-laws in figure 10 for grit and fine glass do not coincide, they do seem to have the same exponent α. In other words, the numerical coefficient λ is a function, $\lambda(\delta, \phi)$, of the material properties, but the exponent α is not. This result again contradicts the conclusions of Lube *et al.* (2004) who claim to see no such dependence. However, they used materials with similar internal angles of friction (and presumably also basal friction angles) whereas we have considered materials with very different frictional properties. Indeed, had we added data for coarse glass and polystyrene to the figure, they would have overlain points for fine glass.

Figure 10 also hints that the sand data depend on more than just the aspect ratio a: the results for $L = 2$ behave slightly differently to the rest ($L > 2$). This is more apparent in a plot of the scaled runout measured from the gate, $(l_\infty - L)/L$, against

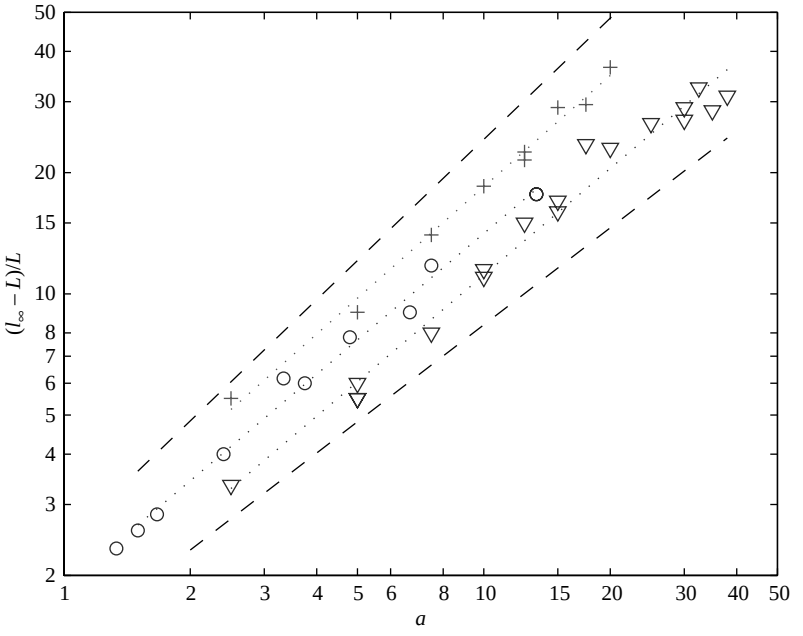

FIGURE 11. The scaled runout from the gate $(l_\infty - L)/L$ plotted against a for grit ($\circ$, $L > 2$; $\triangledown$, $L = 2$) and fine glass ($+$, all with $L = 2$ cm) in the wide slot. The dotted lines represent best fits through the data with gradients of 0.88 (grit $L = 2$ and $L > 2$) and 0.92 (fine glass). The dashed lines are guide lines with gradients of 0.8 and 1 to indicate that the gradient of the data is approximately 0.9 ± 0.1.

a (see figure 11). The data is not so clean here and

$$\frac{(l_\infty - L)}{L} \sim \lambda a^\alpha, \tag{4.2}$$

where $\alpha = 0.9$ with an error of ± 0.1. Again the numerical coefficient is material dependent, $\lambda = \lambda(\delta, \phi)$, but there is also a noticeable dependence on L, or rather on the second length scale ratio, $b := W/L$, in the problem after $a := H/L$.

4.2. *Fractured profiles*

Smaller initial columns develop a slip surface along which the medium initially fractures. This leaves a portion of the mass near the wall that does not move in the slump (these are the leftmost data points in figure 10). In figure 12, we show results for grit dam breaks in the box with lifting gate; the geometry of the box ensures fractured deposits in these experiments. The profiles can be scaled to remove much of the difference between the individual slumps by using the initial height to scale depths, and the final runout measured from the original position of the gate (x_g), to scale horizontal lengths, i.e. by plotting h/h_∞ against $(x - x_g)/(l_\infty - x_g)$. This scaling is suggested by the theoretical results of § 6, and indicates that the fractured deposits have a nearly universal shape. Indeed, by performing the same reduction on the data from experiments in the wide slot (figure 13), we recover practically the same curve. Because the initial placement in the box is much looser than in the slot, the agreement further suggests that the initial packing does not play a significant role in determining the final shape, unlike in the experiments by Daerr & Douady (1999). What differences

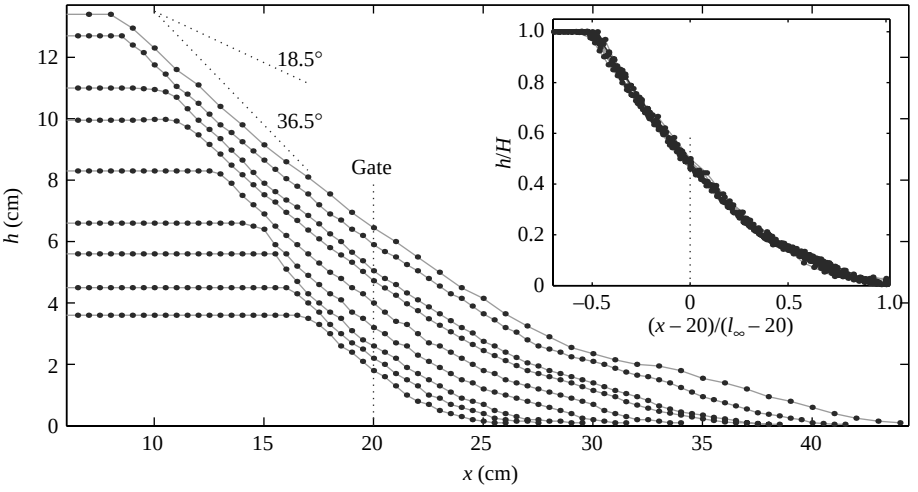

FIGURE 12. Final profiles of slumps of grit in the box (with $W = 18$ cm). The inset shows the results when the profiles are scaled such that depths are normalized by the initial height and horizontal lengths so that the runout from the gate is unity.

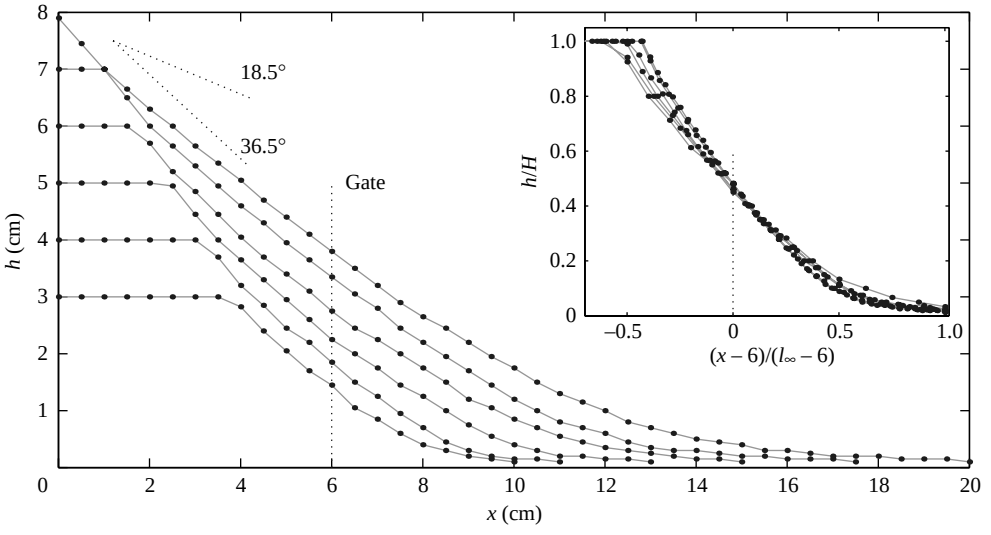

FIGURE 13. Final profiles of slumps of grit in the wide slot; similar plot to figure 12.

remain between the insets of figures 12 and 13 might be attributable to initial packing effects, but could also reflect the influence of the channel width ($b = W/L$),

5. Collapses in the narrow slot

Experiments varying the initial length L and height H, but fixing the volume of the initial column are shown in figures 14 and 15. The final deposit has a shape that is roughly independent of the initial aspect ratio, except near the nose of the deposit where depth systematically decreases as L increases. We interpret this to indicate that the higher thinner initial columns gained more kinetic energy as they fell, thus running

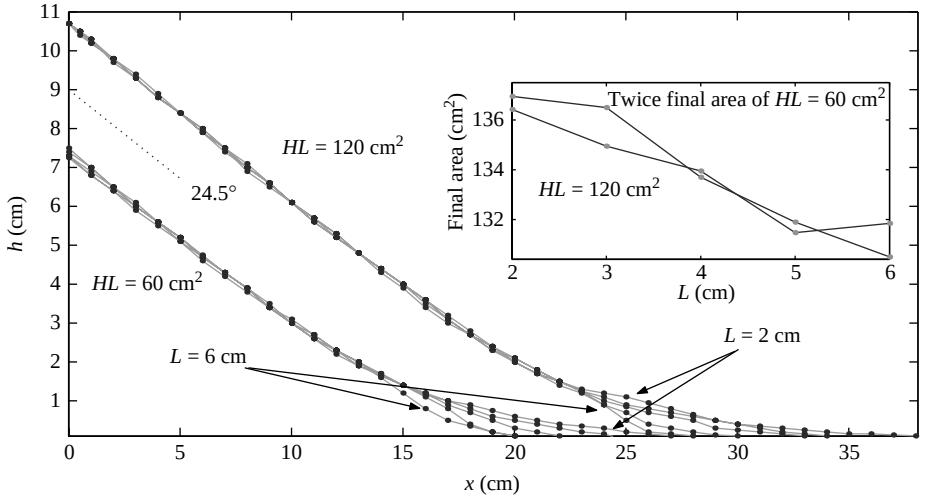

FIGURE 14. Final profiles: fine glass beads, varying initial length at fixed volume in a narrow slot (1 cm).

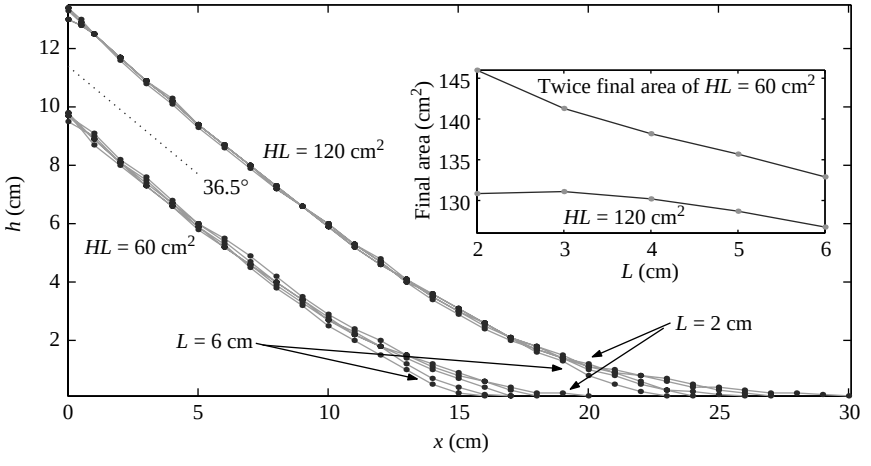

FIGURE 15. Final profiles: grit, varying initial length at fixed volume in a narrow slot (1 cm).

out further and becoming less packed at their noses. The reduction in packing is also seen in the comparison of final areas.

A compendium of profiles for fine glass and grit with fixed initial length L and increasing initial height H is shown in figures 16 and 17. Once these profiles are scaled by final maximum height, h_∞, all the profiles collapse fairly well onto a single curve, suggesting that there is an underlying universal profile characterizing these collapses. As also illustrated in the figures, the slopes near the end of the slot now match closely with the internal angle of friction: the bed angle seems to characterize little of the final deposit. Given that sidewall friction (which is measured by the basal friction angle δ since the wall and base are both Perspex) ought now to be a dominant influence, this is surprising. We return to the issue in § 6 after an evaluation of the theoretical model.

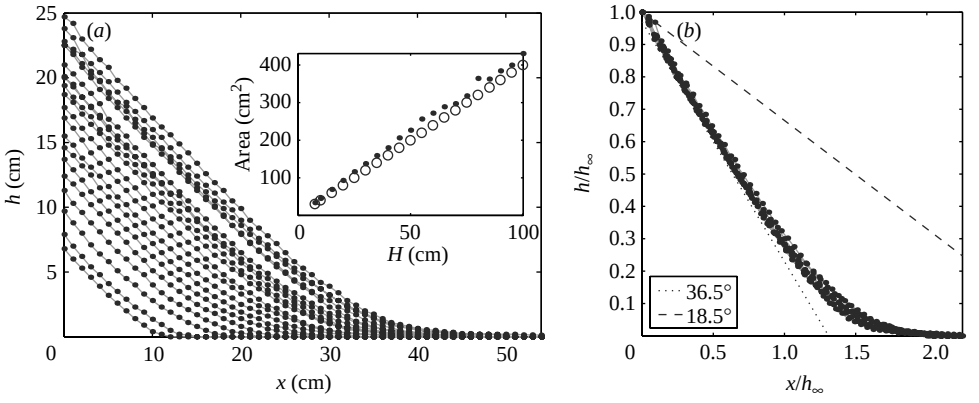

FIGURE 16. Final profiles for grit in the narrow slot. (*a*) The raw data, and (*b*) the data with length scaled by h_∞. The inset in (*a*) compares the initial (○) and final (●) areas. The extra lines in (*b*) illustrate the internal and bed friction angles.

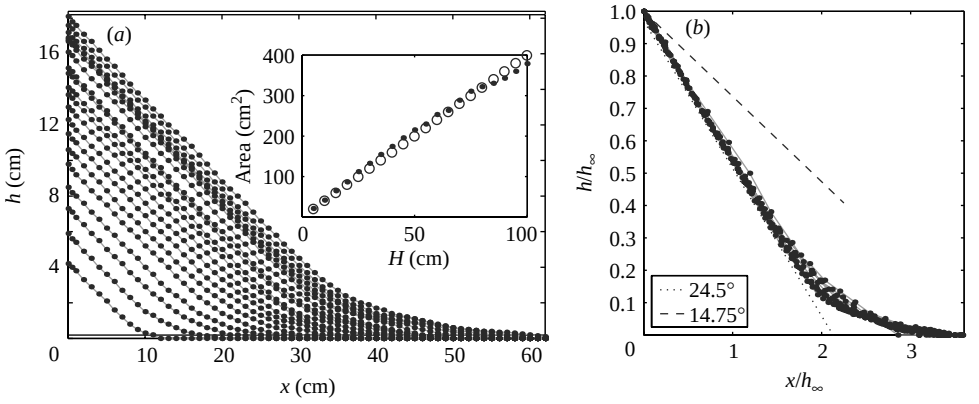

FIGURE 17. Final profiles for fine glass in the narrow slot; similar plotting scheme to figure 16.

Figure 18 indicates that the initial to final height ratio H/h_∞ is well fitted by the power law,

$$\frac{H}{h_\infty} \sim \lambda a^{0.5}. \tag{5.1}$$

As in the wide slot (see figure 10), the best fits for grit and fine glass have the same exponent, but a material-dependent numerical pre-factor. Also as before, the runout data ($(l_\infty - L)/L$ plotted against a in figure 19) is less clean. Adopting a power-law relationship,

$$\frac{(l_\infty - L)}{L} \sim \lambda a^{\alpha}, \tag{5.2}$$

implies $\alpha = 0.65 \pm 0.05$, with a material-dependent numerical coefficient. Given the success of renormalizing the final profiles with the final height (see figures 16 and 17), l_∞/L was also plotted against a (not shown). The plot looks very similar to figure 19, but now the best fits have exponents much closer to the scaling exponent for H/h_∞.

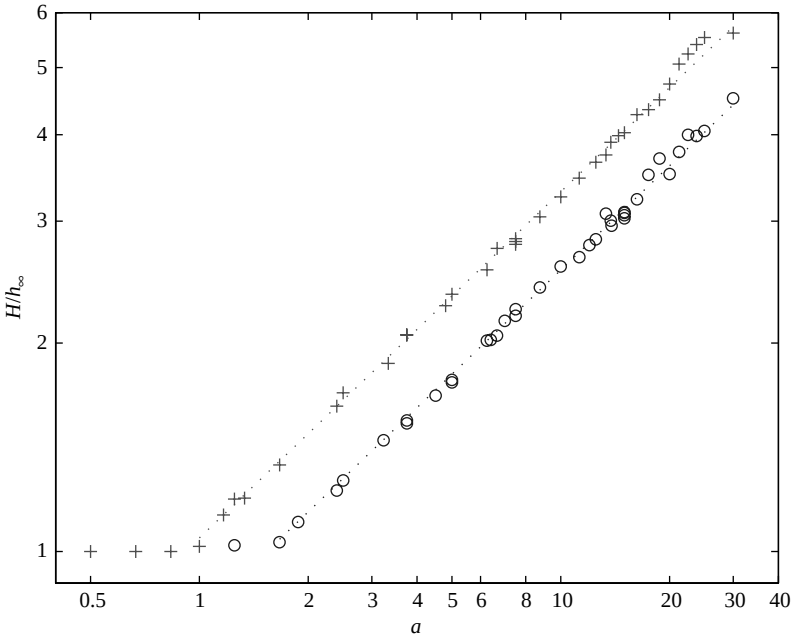

FIGURE 18. The initial to final height ratio H/h_∞ plotted against a for grit ($\circ$) and fine glass ($+$) in the narrow slot. The dotted lines are fits through the data with gradients of 0.5.

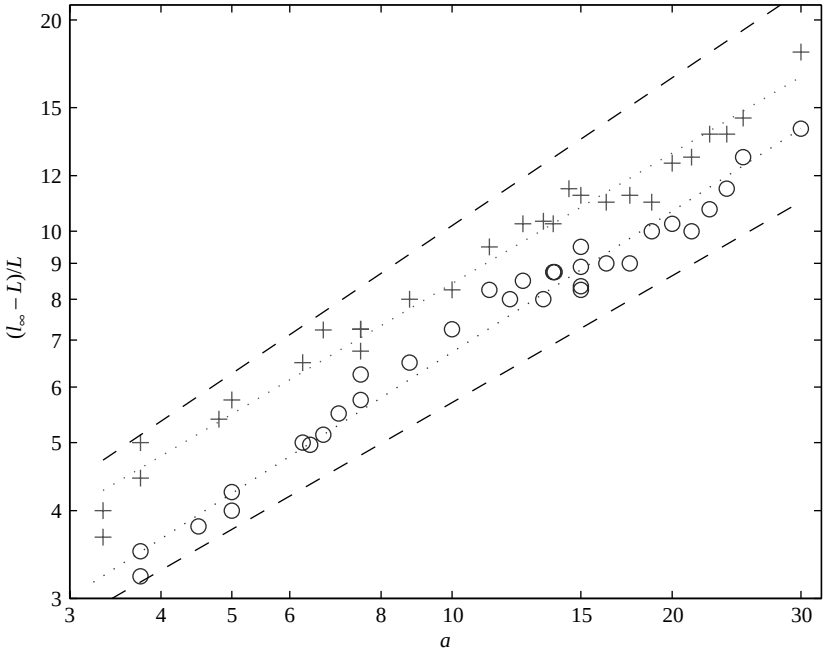

FIGURE 19. The scaled runout from the gate $(l_\infty - L)/L$ plotted against a for grit ($\circ$) and fine glass ($+$) in the narrow slot. The dotted lines represent best fits through the data with gradients of 0.67 (sand) and 0.62 (fine glass). The dashed lines are guide lines with gradients of 0.6 and 0.7 to indicate that the gradient of the data is approximately 0.65 ± 0.05.

Specifically, we find the best fit power laws,

$$\frac{l_\infty}{L} \sim \lambda a^{0.55\pm0.05}. \tag{5.3}$$

Hence, $h_\infty l_\infty/(HL)$ has, at best, a very weak dependence on a which is consistent with figures 16 and 17.

6. Comparison with a simple theory

6.1. *A two-dimensional model*

We now compare the experimental results with a simple theory idealizing the granular material as a shallow fluid layer in which frictional sliding along the base provides a key resistance to flow. Some details of how such a model can be derived asymptotically from the governing fluid equations with a suitable constitutive law for the internal and frictional stresses are given in the Appendix. We arrive at a model that is similar to that proposed by Savage & Hutter (1989).

The model can be conveniently written in terms of the fluid depth, $h(x,t)$, and horizontal speed, $u(x,t)$, and takes the form,

$$h_t + (hu)_x = 0 \tag{6.1}$$

and

$$u_t + uu_x = -g\,\mathrm{sgn}(u)\tan\delta - gKh_x, \tag{6.2}$$

where the fluid density is ρ, g is gravity, and, as above, δ is the bed angle of friction. Also, K is a constant coefficient whose value depends on the basal and internal angles of friction and whether the flow is converging or diverging (active or passive; see Appendix). In the Appendix, we derive the expression

$$K = K_g = \frac{1-\sigma\sin\phi}{1+\sigma\sin\phi}, \tag{6.3}$$

where $\sigma := \mathrm{sgn}(u_x) = u_x/|u_x|$, based upon one particular choice of constitutive model for the granular medium. An alternative form is suggested by the Mohr–Coulomb model of Savage & Hutter:

$$K = K_s = \frac{2}{\cos^2\phi}\left(1-\sigma\sqrt{1-\frac{\cos^2\phi}{\cos^2\delta}}\right) - 1. \tag{6.4}$$

Note that (6.4) can be reduced to (6.3) in the limit $\delta \ll 1$, which is a key condition under which the model is derived in Appendix A.

The equations have a special 'balanced' equilibrium profile with a constant slope in which the bed friction exactly counters the gravitational stress: $\tan\delta = -Kh_x$. Should the inclination of the surface of a granular mass be larger than this slope, the fluid accelerates; where the slope is less, the fluid speed decelerates. However, after a dam break, the balanced profile is not the final realized deposit. Instead, the gravitational driving pushes material sideways, forcing the surface inclination to decline towards the critical slope, but then inertia carries the material beyond that critical slope to form shallower deposits. The importance of inertia can therefore be judged by the departure from the balanced slope. This is likely to be most important at the leading edge of the deposit, and least important near the back wall of the slot. However, a detailed understanding of the final shape requires us to solve the model as an initial-value problem, starting at the instant of release and ending when the material finally comes to rest.

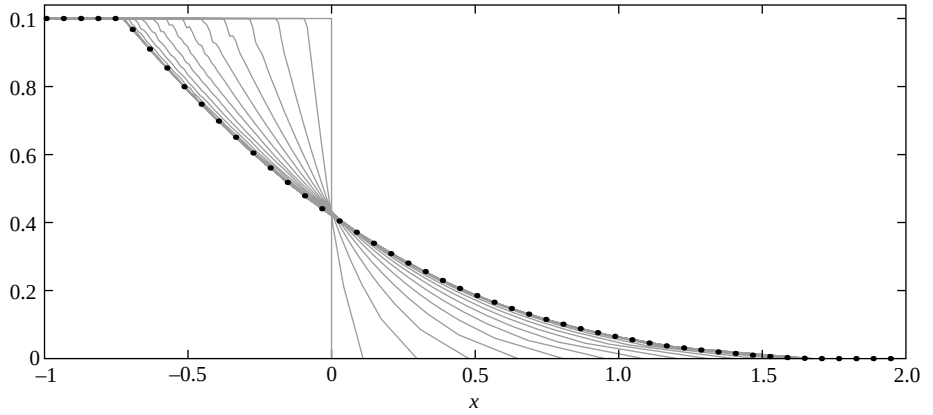

FIGURE 20. Theoretical slump with $A = 1$. The main panel shows snapshots of the collapsing thickness field, spaced by 0.2 time units. The points show the final profle.

Provided that $u > 0$ and u_x remains one-signed, a scaling of lengths, speed and time ($h = H\hat{h}$, $x = HK\hat{x}\cot\delta$, $u = \hat{u}\sqrt{gHK}$ and $t = \hat{t}\sqrt{HK/g}\cot\delta$, plus dropping the hat decoration after the rescaling) can be used to place (6.1)–(6.2) into the form,

$$h_t + (hu)_x = 0 \tag{6.5}$$

and

$$u_t + uu_x + h_x = -1, \tag{6.6}$$

with initial and boundary conditions,

$$h(x,0) = \begin{cases} 1 & -1/A \leqslant x \leqslant 0, \\ 0 & x > 0, \end{cases} \qquad u(0,t) = 0, \tag{6.7}$$

where the slot occupies the region $-1/A \leqslant x$, the gate lies at $x = 0$ and

$$A := \frac{aK}{\tan\delta} \tag{6.8}$$

is the renormalized initial aspect ratio (the only remaining parameter). This system can be attacked effectively (and semi-analytically) using the method of characteristics; further details are provided by Kerswell (2005). The initial assumptions on u and u_x are realized in the solutions for all time ($\mathrm{sgn}(u) = \mathrm{sgn}(u_x) = +1$), and so the calculations are self-consistent, despite the discontinuous coefficients of the original equations.

Depending on the initial aspect ratio, two possible situations arise, as illustrated in figures 20 and 21. For both, the release of the pile spawns a characteristic from $x = 0$ that propagates to the right and marks the leading edge of the fluid. The space–time curve of this front is given by $x_f = t(2 - t/2)$. After a time $t = 2$, the leading edge comes to a stop at $x = 2$, at which point the slump as a whole is at rest. The initial release also spawns a more slowly moving, back-propagating characteristic which comes to rest before the leading edge. If the backwards characteristic does not reach the end of the slot ($x = -1/A$), the deposit forms a fractured type of profile and the maximum final height remains equal to the initial height (figure 20). However, if the characteristic reaches the slot's end, it reflects back from the rear wall at $x = -1/A$ and the entire layer participates in the slump (figure 21). The reflected characteristic eventually halts somewhere between the nose and the back wall, where it scars the final deposit with an abrupt change in surface slope.

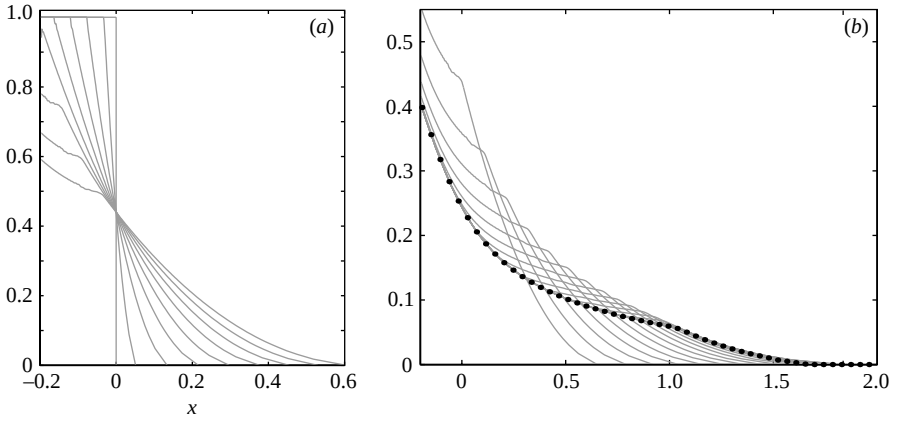

FIGURE 21. Theoretical slump with $A = 5$. Snapshots of the collapsing thickness field; in (a), the snapshots are 0.048 time units apart, and in (b), they are twice that. The points in (b) show the final profle.

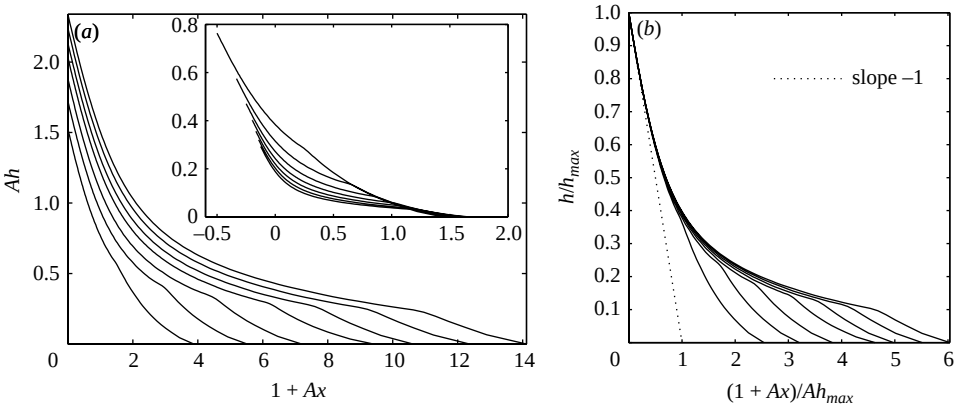

FIGURE 22. Final profiles of theoretical computations for various initial aspect ratios in cases in which the entire initial column slumped. $A = 2$, 3, 4, 5, 6, 7 and 8. The length and depths are rescaled to show the results in a similar fashion to the raw experimental data with fixed initial length L, as figures 8(a) and 9(a). The inset shows the unscaled profiles. In (b), the lengths and depths are scaled by the final maximum thickness, as in figure 8(b) and 9(b). In both panels, as aspect ratio decreases, the profiles extend further to the right.

Figure 22 shows a compendium of final profiles for varying initial aspect ratio, and figure 23 displays the evolution of maximum height and runout. Because of the scaling reducing (6.1)–(6.2) to (6.5)–(6.6), the initial column in the solutions has unit height and the position along the slot has its origin at the gate. To present the results in a similar fashion to the experimental data, we rescale the profiles and shift x in figure 22(a) ($h \to Ah$ and $x \to 1 + Ax$; the inset shows the original solutions). Figure 22(b) shows how the profiles can then be scaled by the final maximum height, much as we dealt with the experimental data.

6.2. *Comparison with the wide slot*

The evolutionary trends displayed in figures 20 and 21 reproduce aspects of the behaviour seen in the experiments in the wide slot and box (i.e. the fracturing of

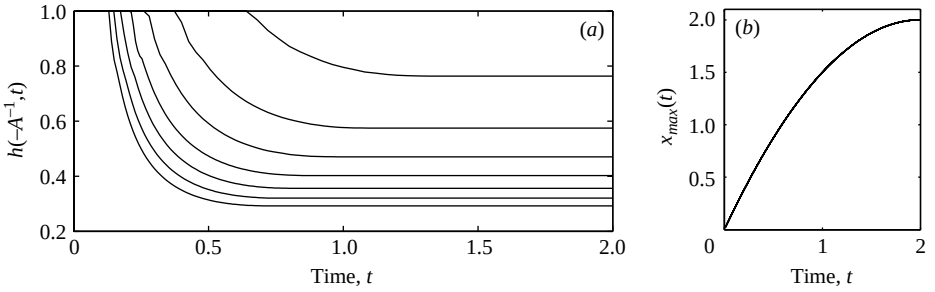

FIGURE 23. Time series of (a) maximum height and (b) instantaneous runout for the computations of figure 22. ($A = 2$, 3, 4, 5, 6, 7 and 8, with the largest A slumping furthest.) In (b), all the data collapse on to the curve $x = x_f(t) = t(2 - t/2)$.

lower initial piles or complete slumping of higher initial columns). The final profiles shown in figure 22 also compare well with the experimental results displayed in figures 8 and 9. This agreement is remarkable given that the theory is based on a shallow-layer expansion, yet the initial experimental columns are much taller than they are wide and far from a shallow limit (more possible errors are mentioned in Appendix A). In actual fact, there are quantitative disagreements between theory and experiment that can be seen on a closer examination of the results.

From figure 22(b), we see that the slope at the end of the slot for completely slumped columns approaches -1 when h and x are scaled by the final maximum height. In terms of the original variables of (6.1)–(6.2), that limiting value corresponds to an actual slope of $K^{-1}\tan\delta$. In other words, near the end of the channel, the final profiles limit to the 'balanced equilibrium profile' whose slope is determined by a combination of both angles of friction. We may easily calculate the balanced angle given the data in table 1 for our granular media. According to (6.3), derived in the Appendix, the limiting angle should be 52° for the grit and 32° for the fine glass (given that $\sigma = +1$). Alternatively, for the Savage–Hutter model, from (6.4), these two angles are predicted to be 36° and 24°, respectively, and are close to the values expected for $K = 1$ which has also been advocated in the past (e.g. Pouliquen & Forterre 2002). None of these estimates compare well with the experimental observations, which lie somewhere between the bed and internal angles of friction for both materials (and are about 23° and 18°, respectively), although the values expected from the Savage–Hutter model are certainly closer. However, in view of the crudeness of the theory, it seems unwarranted to make a definite choice for this special angle, based on a particular theoretical model.

Instead, we opt for an empirical choice for K, or, equivalently, of $K^{-1}\tan\delta$. Unfortunately, even this choice is ambiguous since there are various ways to make the selection, and the different choices are not in agreement. The choices ultimately reflect different dominating errors in the theory. For example, one obvious choice is given by the limiting final slope at the end of the slot. In this case, the theoretical estimates may suffer because of a poor representation of the constitutive and sliding behaviour of the material, or because the shallow-layer approximation fails to represent the limiting stress distributions of the final deposit sufficiently accurately (indeed, the 'small' parameter ϵ, the aspect ratio, used in the reduction is not particularly small).

A second choice can be based on the aspect ratio that divides initial piles which completely slump from those that fracture and $H = h_\infty$ (that is, the aspect ratio for which the maximum final height is no longer the initial height). Theoretically, this happens for a specific choice of A, the rescaled aspect ratio. Experimentally,

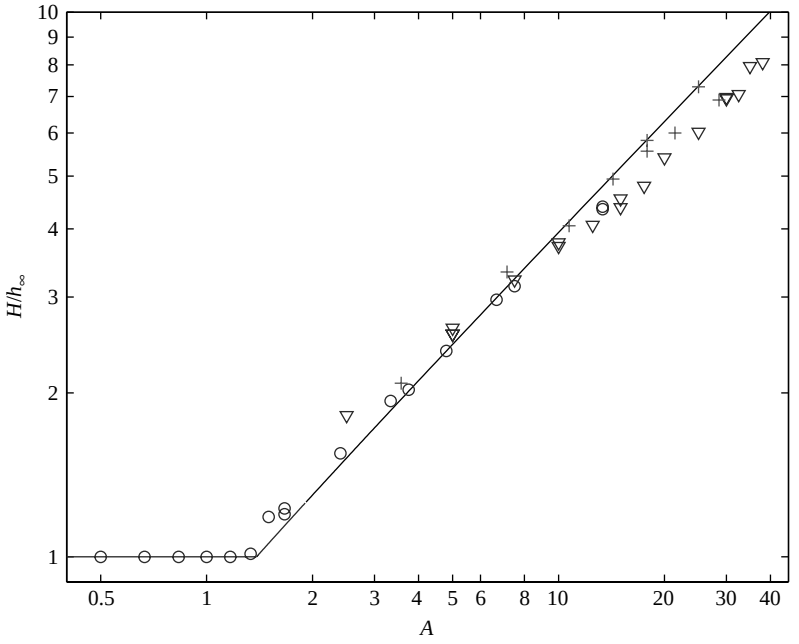

FIGURE 24. The theoretical prediction for H/h_∞ as a function of A (solid line; from Kerswell 2005) in the wide slot plotted with grit data (○, $L > 2$; ▽, $L = 2$) and fine glass data (+). To obtain A from a for the data, the best choice for $\tan\delta/K$ was made: $\tan 45^\circ$ for grit and $\tan 35^\circ$ for fine glass (these choices shift the data as a whole across the plot so they align at the bifurcation point where H/h_∞ leaves the value 1).

we measure the actual aspect ratio, a, for which this division occurs for each of the granular materials. By using (6.8), we then find that $\tan\delta/K \approx \tan 45^\circ$ for grit, whereas $\tan\delta/K \approx \tan 35^\circ$ for fine glass. These compare poorly with the previous estimates. The theoretical error, in this instance, surely lies in the fact that the initial phases of the collapse are governed by physics not captured in the shallow-layer model (such as vertical acceleration) because the initial aspect ratio is not at all small (in fact it exceeds unity). At best, it is only after an initial transient that the theory captures the dynamics, and A should then be redefined in some manner to reflect the aspect ratio when the theory becomes valid (Larrieu *et al.* 2005, in fact, extend the shallow-layer model in such directions).

Guided by this, we use the second choice for K to compare the predicted final heights and runouts with the experimental scaling laws uncovered earlier. In terms of A, the model predicts the scaling laws,

$$\frac{H}{h_\infty} \sim A^\alpha, \tag{6.9}$$

where $\alpha \approx 0.69$ at $A = 5$ decreasing down to $\alpha \approx 0.67$ at $A = 50$ (and ultimately 2/3 as $A \to \infty$), together with

$$\frac{(l_\infty - L)}{L} = 2A \tag{6.10}$$

(see Kerswell 2005 for details). These results are compared with the experimental data in figures 24 and 25. Agreement for the initial and final height ratio is only partial because the data show a weaker dependence on a ($H/h_\infty \sim a^{0.6}$ rather than

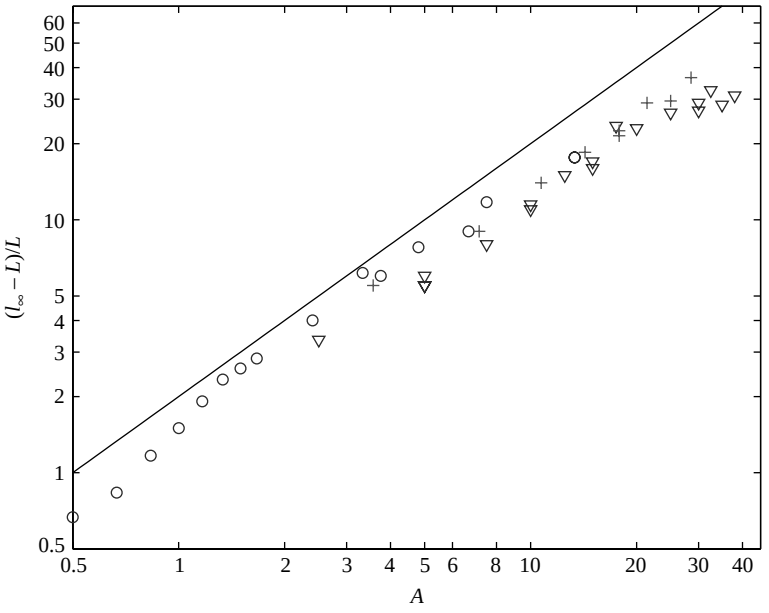

FIGURE 25. The theoretical prediction, $(l_\infty - L)/L = 2A$, (solid line; from Kerswell 2005) in the wide slot plotted with grit data ($\circ$, $L > 2$; $\triangledown$, $L = 2$) and fine glass data (+). To be consistent with figure 24, the same values for $\tan\delta/K$ ($\tan 45^\circ$ for grit and $\tan 35^\circ$ for fine glass) were used to convert the data over a to that over A.

$H/h_\infty \sim a^{0.67}$). The runout comparison shown in figure 25 confirms that the model performs fairly well there too, but again the scaling exponent is not quite captured (data $\sim a^{0.9\pm0.1}$ rather than $\sim a$).

Another useful measure of slumped fractured profiles is suggested by the characteristics solution. For a fractured deposit, the material falls at the gate to a depth, $h_f \approx 0.4229H$, and the slump propagates back a (scaled) distance, $l_f \approx 0.7216$. These predictions do not depend on the empirical choice of K and so offer an independent test of the theory. Experimental measurements of depth at the gate (as seen in figures 12 and 13) suggest

$$\frac{h_f}{H} = \begin{cases} 0.44 - 0.50 & \text{grit, box,} \\ 0.45 - 0.49 & \text{grit, wide slot,} \\ 0.44 - 0.49 & \text{polystyrene, fine and coarse glass, box,} \\ 0.40 - 0.43 & \text{fine glass, wide slot,} \end{cases}$$

which are a little high, but not uncomfortably so. The theoretical ratio of l_f to the forward runout from the gate (2 in scaled units) is 0.3608, which can also be compared with the data shown in figures 12 and 13. The experimental ratio is clearly much closer to 0.5. However, as remarked earlier, the runout is probably our worst experimental measurement. Moreover, our actual measurement of the runout is based on where the medium has a finite thickness (of 2 mm or so), which clearly underestimates the runout, and so the experimental values of $l_f/(l_\infty - L)$ should be larger than expected theoretically.

Although the comparison of the theoretical and experimental final profiles described so far is not too discomforting, there are more significant disagreements in the evolutionary dynamics. First, the evolving profiles of figures 20 and 21 do not

compare favourably with the more complicated shapes photographed in figure 2. Secondly, as seen in the time series of figure 23, when the entire pile slumps, the initial fall of material at the wall is always relatively sharp. By contrast, in the experiments with higher initial columns, there is a clear ballistic behaviour at the outset (see figure 5) and the collapse proceeds more smoothly. Much of these discrepancies could again result from the absence of vertical accelerations in the shallow-fluid model, although some of the other possible flaws in the theory mentioned in Appendix A may contribute.

6.3. *The narrow slot*

When the granular medium slides in a slot, the walls introduce an additional source of friction. By proceeding as in Appendix B, we generalize the shallow-layer model (6.1)–(6.2) as follows:

$$h_t + (hu)_x = 0, \tag{6.11a}$$

$$u_t + uu_x = -g(1 + \Lambda h)\,\mathrm{sgn}(u)\,\tan\delta - gKh_x, \tag{6.11b}$$

where Λ is a friction coefficient which, for the particular constitutive law used, takes the value,

$$\Lambda = [W(1 + \sigma \sin\phi)]^{-1} \tag{6.12}$$

(cf. Hutter & Koch 1991). Evidently, the higher the deposit, the more contact with the walls of the slot and the greater the friction.

Computations with the model in (6.11*b*) suggest a similar dynamics to that presented above without sidewalls. In particular, when the whole initial column slumps, the final shape at the end of the slot approaches the balanced equilibrium profile, which is dictated by

$$Kh_x = -(1 + \Lambda h)\tan\delta \qquad \text{or} \qquad h = \frac{1}{\Lambda}\left[(1 + \Lambda h_0)\mathrm{e}^{-x(\Lambda/K)\tan\delta} - 1\right]. \tag{6.13}$$

At the wall, the balanced slope, $-(1 + \Lambda h_0)\tan\delta/K$, increases with depth, illustrating the enhancement of surface slopes by sidewall friction.

At this stage, we observe a striking disagreement between experiment and the theoretical prediction. In contrast to (6.13), the observed final profiles in the narrow slot show no significant dependence on height (e.g. see figures 16 and 17). At the heart of this discrepancy is the fact that the theoretical model is based on the assumptions that $\tan\delta \ll 1$ and $|h_x| \ll 1$, but ϕ remains order one. The balanced profile, on the other hand, predicts that $h_x \sim -\Lambda h \tan\delta$ for $\Lambda \gg 1$. That is, the slope grows exponentially for large sidewall friction, which ultimately will violate the condition, $|h_x| \ll 1$. Indeed, the experiments show a slope of $-\tan\phi$ near the end of the slot, which is of order unity and therefore already out of the range of validity of the theory. To model the slump for $O(1)$ surface slopes, we must return to a more general form of the fluid equations (see Appendix B). The solution of these 'slot equations' is out of the scope of the present paper, and so we close the theoretical discussion by mentioning a simple fix for the theory when the surface slopes become too large.

A key feature of the sidewall friction is its dependence on ambient pressure: for a narrow slot with Coulomb-type slip conditions, the (x, z)-components of friction are given by

$$\frac{2}{W} p \tan\delta \frac{(u, w)}{\sqrt{u^2 + w^2}}, \tag{6.14}$$

where w is the vertical velocity. In the fluid interior, these frictional terms may become sufficiently large to hold the material in place and prevent basal sliding, even if the surface slopes are relatively steep. By contrast, since the pressure vanishes on the surface, the superficial layers experience little sidewall friction. As a result, their stability is determined by the angle of repose: should the inclination of the free surface exceed the internal angle of friction, the surface layers fail by avalanching over the layers beneath to form a shallower deposit. This kind of failure produces a surface-confined current with a static interior, a flow configuration that cannot be captured by the plug-like structure of velocity field in the thin-layer model. Furthermore, this dynamics matches precisely the phenomenology of the narrow-gap experiments, where secondary surface avalanching was often seen.

Assuming that surface failure occurs whenever $|h_x| > \tan\phi$, we arrive at a simple prescription for limiting surface slopes:

$$h_x = -\min[K^{-1}(1 + \Lambda h)\tan\delta, \tan\phi]. \tag{6.15}$$

This formula bridges between slopes at the angle of repose for deeper deposits, and slopes for thinner layers nearer the balanced profile expected for two-dimensional slumps. The cross-over between the two limits occurs for depths of order $[K\tan(\phi)/\tan(\delta) - 1]/\Lambda$. For our narrow slot, this depth is about a centimetre for both grit and sand, and so most of the profile would fall along the angle of repose, as observed. Conservation of mass then leads to

$$l_\infty/L \approx \sqrt{2a/\tan\phi} \approx H/h_\infty, \tag{6.16}$$

which captures the observed final maximum height scaling and marginally underestimates the observed runout scaling.

7. Discussion

We have performed two-dimensional dam-break experiments for granular materials in a channel, characterizing the slumps largely by the final deposit. We have also offered a theoretical model that appears to capture several (but not all) aspects of the dynamics. As with axisymmetric collapses (Lajeunesse *et al.* 2004; Lube *et al.* 2004), there is some evidence that the final height and runout of the slumped deposit can be represented by power-law dependences on the initial aspect ratio, a. The data are particularly clean for the final height and argue for

$$\frac{H}{h_\infty} \sim a^{0.6} \quad \text{(wide slot)}, \qquad \frac{H}{h_\infty} \sim a^{0.5} \quad \text{(narrow slot)}, \tag{7.1}$$

whereas the runout data show more scatter and suggest that

$$\frac{l_\infty - L}{L} \sim a^{0.9\pm0.1} \quad \text{(wide slot)}, \qquad \frac{l_\infty - L}{L} \sim a^{0.65\pm0.05} \quad \text{(narrow slot)}. \tag{7.2}$$

Another characterization of the runout data in the narrow slot,

$$\frac{l_\infty}{L} \sim a^{0.55\pm0.05}, \tag{7.3}$$

backs up the finding that the narrow-slot final profile seems to display a universal shape ($h_\infty l_\infty/HL$ is essentially independent of a). Surprisingly, the final height exponents do not depend on the material used (this finding probably carries over to the runout scalings, but the data are not good enough to support this conclusion).

The numerical constants of proportionality, however, show clear material dependence. This corroborates the conclusion of Lajeunesse *et al.* (2004) and softens that of Lube *et al.* (2004).

By way of comparison, the shallow-layer model used here predicts

$$\frac{H}{h_\infty} \sim a^{0.67}, \qquad \frac{l_\infty - L}{L} \sim a \tag{7.4}$$

for the wide-slot experiments. The narrow-slot version of the theory produces steep final deposits which we conclude undergo secondary avalanching until the slope corresponds to the angle of repose. This predicts that

$$\frac{H}{h_\infty} \sim a^{0.5}, \qquad \frac{l_\infty}{L} \sim a^{0.5}, \tag{7.5}$$

which is in fair agreement with observations.

The distinction between what constitutes a 'wide' or a 'narrow' slot requires some discussion. For axisymmetric releases, there are only three, dimensional quantities which enter the problem (ignoring the internal properties of the granular material such as the particle diameter†): the height H and radius R of the initial cylinder and g, the acceleration due to gravity. Once the problem has been non-dimensionalized by choosing a length and time scale, this leaves just one non-dimensional parameter, $a := H/R$ the aspect ratio, upon which the solution can depend. As a result, the final height h_∞, for example, can be written as $h_\infty = H\, f(a)$ for some unknown function, $f(a)$. Lajeunesse *et al.* (2004) and Lube *et al.* (2004) suggest that $f(a)$ is a power law, λa^α. The channel problem studied in this paper, however, has an extra lengthscale, the width W, and hence a second non-dimensional parameter, $b := W/L$, upon which the solution can depend. Following the same line of thinking, we can expect $h_\infty = H\, f(a, b)$ where f is a new unknown function. The original motivation behind our narrow- and wide-slot experiments was to examine the large and small b behaviour of f with the idea of seeing if these limits also had a simple power-law structure. That is, whether

$$f(a, b) \approx \begin{cases} \lambda_1 a^{\alpha_1}; & b \to \infty; \quad \text{wide slot,} \\ \lambda_2 a^{\alpha_2}; & b \to 0; \quad \text{narrow slot,} \end{cases} \tag{7.6}$$

which is, indeed, suggested by our results. The scaling of the runouts are less impressive but, in truth, it is unclear whether the problem lies with the actual data measurements or in the power-law assumption. What undoubtedly emerges, however, is that slumping experiments in two-dimensional channels depend on the channel width. Assuming that the scaling exponents for the final height and runout are simple monotonic functions of b, we can (minimally) expect the exponent of the power laws for H/h_∞ and $(l_\infty - L)/L$ to vary across the ranges $[0.5, 0.6]$ and $[0.6, 1]$, respectively.

It is clear that there is much still to be learnt from this experimental set-up. The fact that power laws can be used to describe the final deposit has been confirmed for two-dimensional slumping. However, these laws are influenced by the presence of sidewalls and depend (albeit only in the numerical coefficent of proportionality) on the frictional properties of the granular material. The theoretical model also exhibits scaling-law dependencies, but not quite those observed. Moreover, the model fails to

† Collapses of coarse glass beads, with diameters of about 3 mm, in the narrow slot, of width 1 cm, give an example in which we do not seem able to ignore effects of particle size.

capture the initial collapse phase and cannot be compared in detail to the observed flow dynamics.

The work was performed at the Geophysical Fluid Dynamics Summer Study Program, 2002 and 2004, Woods Hole Oceanographic Institution, which is supported by N. S. F. and O. N. R. We thank Jack Whitehead for space and equipment in his Lab, Keith Bradley for building the apparatus, and Karl Helfrich for allowing us to make a mess on his laser table.

Appendix A. Shallow-fluid theory

Consider a two-dimensional incompressible fluid described by the momentum equations,

$$\left.\begin{aligned}\rho(u_t + uu_x + wu_z) &= -p_x + \partial_x\tau_{xx} + \partial_z\tau_{xz},\\ \rho(w_t + uw_x + ww_z) &= -p_z - \rho g + \partial_x\tau_{xz} + \partial_z\tau_{zz},\end{aligned}\right\} \tag{A 1}$$

where $\boldsymbol{\tau}$ is the deviatoric stress tensor, p the pressure, ρ the density, g the acceleration due to gravity and (u, w) the velocity components in the (x, z) directions (subscripts denote partial derivatives, except in the case of the stress components). The surface, $z = h(x, t)$, is stress free, whilst at the base $z = 0$, there is no normal flow, $w = 0$, and we impose a Coulomb slip condition (e.g. Nedderman 1992),

$$\tau_{xz} = -(\tau_{zz} - p)\tan\delta\ \mathrm{sgn}(u), \tag{A 2}$$

provided the fluid is stressed sufficiently to slide. We adopt a Herschel–Bulkley-type constitutive model borrowed from viscoplastic fluid mechanics (e.g. Oldroyd 1947),

$$\begin{aligned}\tau_{jk} = \dot\gamma^{-1}(\tau_p + C\dot\gamma^n)\dot\gamma_{jk} \quad &\text{if } \tau \geqslant \tau_y,\\ \dot\gamma_{jk} = 0 \quad &\text{if } \tau < \tau_y,\end{aligned} \tag{A 3}$$

where

$$\dot\gamma_{jk} = \frac{\partial u_j}{\partial x_k} + \frac{\partial u_k}{\partial x_j}, \qquad \tau = \sqrt{\tfrac{1}{2}\sum_{j,k}\tau_{jk}\tau_{kj}}, \qquad \dot\gamma = \sqrt{\tfrac{1}{2}\sum_{j,k}\dot\gamma_{jk}\dot\gamma_{kj}}, \tag{A 4}$$

n and C are constants, and τ_y is the yield stress. Notably, we allow the yield stress to depend on local pressure, $\tau_y = \tau_y(p)$, but otherwise the yield condition is the usual von Mises criterion†. Thus formulated, the model is a viscous generalization of a perfectly plastic Druckner–Prager material (e.g. Davis & Salvadurai 2002), and has common features to the rate-dependent plasticity models considered by Savage and others (see Savage 1984). A particular, useful choice is $\tau_y = \tau_0 + p\sin\phi$, where τ_0 and ϕ are constants that are equivalent to the cohesion and internal angle of friction of the Mohr–Coulomb law (Nedderman 1992).

We remove dimensions as follows:

$$(x, z) = \left(\frac{x}{\epsilon}, z\right)H, \quad t = \frac{\hat t}{\epsilon}\sqrt{\frac{H}{g}}, \quad (u, w) = (\tilde u, \epsilon w)\sqrt{gH}, \quad (p, \tau_{jk}) = (\tilde p, \tilde\tau_{jk})\rho g H, \tag{A 5}$$

† In soil mechanics, the Mohr–Coulomb law with the Tresca yield condition is normally adopted. We choose a different formulation here, although in the shallow limit that we consider, both Tresca and von Mises reduce to the same yield condition. The constitutive model also makes contact with Jenike's materials with 'conical yield functions' (see Nedderman 1992).

where the ratio of vertical and horizontal length scales, ϵ, is assumed small to reach a simplified shallow-layer theory. On dropping the tilde, the momentum equations become

$$\left.\begin{aligned} u_t + uu_x + wu_z &= -p_x + \partial_x \tau_{xx} + \epsilon^{-1}\partial_z \tau_{xz}, \\ \epsilon^2(w_t + uw_x + ww_z) &= -p_z - 1 + \epsilon\partial_x \tau_{xz} + \partial_z \tau_{zz}. \end{aligned}\right\} \tag{A 6}$$

The dimensionless constitutive equation is:

$$\begin{pmatrix} \tau_{xx} & \tau_{xz} \\ \tau_{xz} & \tau_{zz} \end{pmatrix} = \frac{1}{\dot\gamma}\left(B + \frac{\dot\gamma^n}{Re}\right)\begin{pmatrix} 2u_x & \epsilon^{-1}u_z + \epsilon w_x \\ \epsilon^{-1}u_z + \epsilon w_x & -2u_x \end{pmatrix}, \tag{A 7}$$

for $\tau \geqslant B$, or $\dot\gamma_{jk} = 0$ otherwise, with

$$\dot\gamma = \sqrt{4u_x^2 + \epsilon^{-2}(u_z + \epsilon^2 w_x)^2}, \qquad Re = \frac{\rho g H}{C(\epsilon\sqrt{g/H})^n} \tag{A 8}$$

and

$$B(p) = \frac{\tau_y(p)}{\rho g H} \to \frac{\tau_0}{\rho g H} + p\sin\phi \equiv B_0 + p\sin\phi. \tag{A 9}$$

In the problem at hand, the fluid slips over the base at lower stresses than it yields internally (the base is smooth). However, the scaling leading to (A 6)–(A 9), if unchecked, implies that the shear stress, τ_{xz}, dominates, as is typical in thin-layer theories. The predominance of sliding can be built into the shallow-fluid model by requiring the basal friction angle to be small: $\tan\delta \sim \epsilon$. The dimensionless version of the Coulomb sliding law (A 2) can then be written in the form,

$$\tau_{xz} = -(\tau_{zz} - p)\frac{\tan\delta}{\epsilon}\,\mathrm{sgn}(u). \tag{A 10}$$

Now we may take the shear stress to scale as $O(\epsilon)$ and set $\tau_{xz} \to \epsilon\hat\tau_{xz}$. In other words, the fluid slides so easily that the base provides little traction; the shear stress is significantly reduced and the longitudinal stresses emerge in the dominant balance of forces:

$$u_t + uu_x + wu_z = -p_x + \partial_x \tau_{xx} + \partial_z \hat\tau_{xz}, \quad 0 = -p_z - 1 + \partial_z \tau_{zz}, \tag{A 11}$$

to leading order in ϵ, on which we impose the surface stress conditions,

$$p = \tau_{zz}, \quad \text{and} \quad \tau_{xz} = 2h_x\tau_{xx} \qquad \text{on} \quad z = h(x,t). \tag{A 12}$$

A further consequence is that the velocity field must become largely plug-like, $u = u(x,t) + O(\epsilon^2)$, furnishing the constitutive law,

$$\tau_{xx} = \left(B + \frac{|2u_x|^n}{Re}\right)\sigma, \tag{A 13}$$

and yield condition, $|u_x| > 0$, where $\sigma = \mathrm{sgn}(u_x)$.

The vertical momentum balance equation integrates to give

$$p - \hat\tau_{zz} = h - z, \tag{A 14}$$

which leads to an implicit relation for the extensional stress from (A 13). Because our model yield stress has a linear dependence on pressure, this equation may be solved:

$$\tau_{xx} = \frac{\sigma}{1 + \sigma\sin\phi}\left[B_0 + (h-z)\sin\phi + \frac{|2u_x|^n}{Re}\right]. \tag{A 15}$$

The vertical integral of the horizontal momentum equation over the fluid depth, together with the boundary conditions, now gives

$$u_t + uu_x = -h_x + \frac{2}{h}\partial_x(h\overline{\tau_{xx}}) - \frac{\tan\delta}{\epsilon}\,\mathrm{sgn}(u), \tag{A 16}$$

where

$$\overline{\tau_{xx}} = \frac{1}{h}\int_0^h \tau_{xx}\,\mathrm{d}z \to \frac{\sigma}{1+\sigma\sin\phi}\left[B_0 + \tfrac{1}{2}h\sin\phi + \frac{|2u_x|^n}{Re}\right]. \tag{A 17}$$

Finally, the integral of continuity and the kinematic surface condition provide the mass conservation relation, $h_t + (hu)_x = 0$, and we arrive at a model comprised of two partial differential equations dictating $h(x,t)$ and $u(x,t)$. For constant yield stress, $B = B_0$, this reduced model is the inertial sliding generalization of the lubrication theories of Liu & Mei (1989) and Balmforth & Craster (1999) used to describe mud and lava flow. Without inertia and any yield stress, the model corresponds to MacAyeal's (1987) ice-stream model with a particular sliding law.

On setting $B_0 = 0$ and taking the limit $Re \to \infty$, we emerge with

$$u_t + uu_x = -\left(\frac{1-\sigma\sin\phi}{1+\sigma\sin\phi}\right)h_x - \frac{\tan\delta}{\epsilon}\,\mathrm{sgn}(u), \tag{A 18}$$

which is considered more fully in the main text, where we also return to the original dimensional variables. Thus stated, the reduced system corresponds to the Savage–Hutter model, but with a slightly simpler 'active–passive earth-pressure coefficient' (the coefficient of h_x in the first term on the right-hand side of (A 18); the Savage–Hutter version is quoted in (6.4) of the main text). In fact, with $\delta \ll 1$, the Savage–Hutter coefficient reduces precisely to that contained in (A 18), reflecting a common limit in the yield conditions of the two theories. We could argue that the Savage–Hutter coefficient, being derived using Mohr stress circles for non-shallow layers, is potentially more accurate than that in (A 18) (and corresponds precisely to, somewhat arbitrarily, replacing the coefficient of h_x in (A 18) by that expected for the equilibrium of a wedge-shaped pile). Though appealing, the actual accuracy of this 'improvement' is not clear.

In summary, although we began with a different constitutive model for the granular fluid than those normally considered, we have reduced the governing equations to a Savage–Hutter-type model. Moreover, we performed the reduction asymptotically, which highlights that the theory should be accurate, provided $\epsilon \ll 1$ and the bed be relatively slippery, $\delta \ll \phi$. Unfortunately, neither condition is well satisfied in the experiments, and so cannot expect the theory to be particularly accurate, even if the constitutive behaviour were well represented by (A 4)–(A 4). When ϵ is not small, the model is likely to represent the stresses, and therefore the final shape of the deposit, inaccurately. If δ is not much smaller than ϕ, there is no reason to expect a sliding plug-flow, and internal failure could even occur, allowing avalanching of superficial layers, as observed.

Appendix B. Sliding in a narrow slot

When the granular fluid slides within a narrow slot (with cross-slot coordinate, y), we incorporate the additional friction from the sidewalls, located at $y = \pm W/2$, using

the same Coulomb law. The momentum equations take the dimensionless form,

$$\left.\begin{aligned} &u_t + uu_x + vu_y + wu_z = -p_x + \partial_x\tau_{xx} + \partial_y\hat{\tau}_{yz} + \partial_z\tau_{xz},\\ &\Delta^2(v_t + uv_x + vv_y + wv_z) = -p_y + \Delta\partial_x\tau_{xy} + \partial_y\tau_{yy} + \Delta\partial_z\tau_{yz},\\ &w_t + uw_x + vw_y + ww_z = -p_z - 1 + \partial_x\tau_{xz} + \partial_y\hat{\tau}_{zy} + \partial_z\tau_{zz}, \end{aligned}\right\} \tag{B 1}$$

which can be found on scaling (x, z) and (u, w) by the vertical lengthscale H and velocity scale $U = \sqrt{gH}$, y by the slot width, W, and the cross-slot velocity, v, by ΔU, where $\Delta := W/H$. Pressure and deviatoric stress components have the scale ρgH, except for τ_{xz} and τ_{yz}, which receive an additional factor of Δ (warranting their acquisition of a hat). The Coulomb slip conditions on the sidewalls are

$$(\hat{\tau}_{xy}, \hat{\tau}_{yz}) = \pm(p - \tau_{yy})\Delta^{-1}\tan\delta\,\frac{(u, w)}{\sqrt{u^2 + w^2}} \qquad \text{at } y = \pm\tfrac{1}{2}, \tag{B 2}$$

which force us to assume that $\tan\delta$ is now of order Δ. So far, the procedure is much as before, and the main result is that $p - \tau_{yy}$ is independent of y in the limit $\Delta \to 0$.

In fact, the constitutive law is more demanding: Because $\dot{\gamma}_{xy} = \Delta v_x + \Delta^{-1}u_y$ and $\dot{\gamma}_{xy} = \Delta v_z + \Delta^{-1}w_y$, in terms of the unit U/H, the shear stresses across the slot (τ_{xy} and τ_{zy}) can only be made of order Δ smaller than the remaining stress components (as demanded by the scaling above) if the flow down the slot is plug-like:

$$u = u(x, z, t) + O(\Delta^2), \qquad w = w(x, z, t) + O(\Delta^2).$$

Furthermore, the continuity equation, coupled with the impermeable condition of the sidewalls, then implies that $u_x + w_z = O(\Delta^2)$ and $v = O(\Delta^2)$, which leads us to take $\tau_{yy} = O(\Delta)$ and $\dot{\gamma} = \sqrt{4u_x^2 + (u_z + w_x)^2} + O(\Delta)$. A straightforward averaging across the slot now leads to the dynamical equations for our granular 'slot flow':

$$\left.\begin{aligned} &u_t + uu_x + wu_z = -p_x + \partial_x\tau_{xx} + \partial_z\tau_{xz} - \frac{\Upsilon pu}{\sqrt{u^2 + w^2}},\\ &w_t + uw_x + ww_z = -p_z - 1 + \partial_x\tau_{xz} + \partial_z\tau_{zz} - \frac{\Upsilon pw}{\sqrt{u^2 + w^2}}, \end{aligned}\right\} \tag{B 3}$$

where $\Upsilon := 2\tan\delta/\Delta$, and

$$\begin{pmatrix} \tau_{xx} & \tau_{xz} \\ \tau_{xz} & \tau_{zz} \end{pmatrix} = \frac{1}{\dot{\gamma}}\left(B + \frac{\dot{\gamma}^n}{Re}\right)\begin{pmatrix} 2u_x & u_z + w_x \\ u_z + w_x & 2w_z \end{pmatrix}, \tag{B 4}$$

for $\tau \geqslant B$, and $\dot{\gamma}_{xx} = \dot{\gamma}_{xx} = 0$ otherwise, with

$$\dot{\gamma} = \sqrt{4u_x^2 + (u_z + w_x)^2}, \qquad Re = \frac{\rho gH}{C(U/H)^n}, \qquad B(p) = \frac{\tau_y(p)}{\rho gH}. \tag{B 5}$$

Though we do not explore these equations here, we do mention that the opportunity for the surface of a wedge-shaped deposit to fail by sliding in the direction parallel to the surface can be extracted from them, provided the slope exceeds the internal angle of friction (as introduced to limit surface slopes in § 6.3).

When the flow in the slot is relatively shallow, we may approximate the slot equations still further. We introduce the further scalings $x = \tilde{x}/\epsilon$, $t = \tilde{t}/\epsilon$, $w = \epsilon\tilde{w}$, $\tau_{xz} = \epsilon\hat{\tau}_{xz}$, and $\Upsilon = \epsilon\tilde{\Upsilon}$, then fix $u = u(x, t) + O(\epsilon^2)$. To leading order in ϵ (and dropping the tilde decoration), we then recover (A 11), but with an extra term, $-\Upsilon p\ \mathrm{sgn}(u)$, in the horizontal momentum equation. After an integral over depth, we derive (A 16), but supplemented with the sidewall friction term, $-(\Upsilon/2)(h - 2\overline{\tau_{xx}})\ \mathrm{sgn}(u)$. As before, setting $B_0 = 0$ and taking the limit $Re \to \infty$, leads to (6.11*b*).

REFERENCES

Balmforth, N. J. & Craster, R. V. 1999 A consistent thin-layer theory for Bingham fluids. *J. Non-Newtonian Fluid Mech.* **84**, 65–81.

Bouchaud, J.-P., Cates, M. E., Prakash, J. R. & Edwards, S. F. 1994 A model for the dynamics of sandpile surfaces. *J. Phys.* I **4**, 1383–1410.

Daerr, A. & Douady, S. 1999 Sensitivity of granular surface flows to preparation. *Europhys. Lett.* **47**, 324–330.

Davis, R. O. & Salvadurai, A. P. S. 2002 *Plasticity and Geomechanics*. Cambridge University Press.

Hutter, K. & Koch, T. 1991 Motion of a granular avalanche in an exponentially curved chute: experiments and theoretical predictions. *Phil Trans. R. Soc. Lond.* A **334**, 91–138.

Hutter, K., Koch, T., Plüss, C. & Savage, S. B. 1995 The dynamics of avalanches from initiation to runout. Part II: Experiments. *Acta Mech.* **109**, 127–165.

Lajeunesse, E., Mangeney-Castelnau, A. & Vilotte, J. P. 2004 Spreading of a granular mass on a horizontal plane. *Phys. Fluids* **16**, 2371–2381.

Lajeunesse, E., Monnier, J. B. & Homsy, G. M. 2005 Granular slumping on a horizontal surface. *Phys. Fluids* (submitted).

Larrieu, E., Staron, L. & Hinch, E. J. 2005 Raining into shallow water as a description of the collapse of a column of grains. *J. Fluid Mech.* (submitted).

Liu, F. K. & Mei, C. C. 1989 Slow spreading of Bingham fluid on an inclined plane. *J. Fluid Mech.* **207**, 505–529.

Lube, G., Huppert, H. E., Sparks, R. S. J. & Hallworth, M. A. 2004 Axisymmetric collapses of granular columns. *J. Fluid Mech.* **508**, 175–199.

Lube, G., Huppert, H. E., Sparks, R. S. J. & Hallworth, M. A. 2005 Collapses of granular columns. *Phys. Rev.* E (submitted).

Kerswell, R. R. 2005 Dam break with Coulomb friction: a model for granular slumping? *Phys. Fluids* **17**, 057101.

MacAyeal, D. R. 1987 Large-scale ice flow over a viscous basal sediment: theory and applications to ice stream B, Antarctica. *J. Geophys. Res.* **94**, 4071–4087.

Nedderman, R. M. 1992 *Static and Kinematics of Granular Materials*. Cambridge University Press.

Oldroyd, J. G. 1947 A rational formulation of the equations of plastic flow for a Bingham solid. *Proc. Camb. Phil. Soc.* **43**, 100–105.

Pouliquen, O. & Forterre, Y. 2002 Friction law for dense granular flows: application to the motion of a mass down a rough inclined plane. *J. Fluid Mech.* **453**, 133–151.

Savage, S. B. 1984. The mechanics of rapid granular flows. *Adv. Appl. Mech.* **24**, 289–366.

Savage, S. B. & Hutter, K. 1989. The motion of a finite mass of granular material down a rough incline. *J. Fluid Mech.* **199**, 177–215.

Savage, S. B. & Hutter, K. 1991 The dynamics of avalanches from initiation to runout. Part I: Analysis. *Acta Mech.* **86**, 201–223.

Siavoshi, S. & Kudrolli, A. 2005 Failure of a granular step. *Phys. Rev.* E **71**, 051302.

Staron, L. & Hinch, E. J. 2005 Study of the collapse of granular columns using DEM numerical simulation. *J. Fluid Mech.* (in press).

Whitham, G. B. 1974 *Linear and Nonlinear Waves*. Wiley.